Fully Probe-Corrected Near-Field Far-Field Transformations With Unknown Probe Antennas

Alexander Paulus, *Member, IEEE*, and Thomas F. Eibert, *Senior Member, IEEE*

***Abstract*— According to the electromagnetic uniqueness theorem, the radiation behavior of an antenna under test (AUT) can be recovered from measurements of two tangential components of its radiated fields on an enclosing surface. In practice, measurements conducted in the radiating near-field (NF) of an AUT utilize probe antennas of finite size. Thus, instead of discrete field values, spatially blurred probe signals are acquired. The probe influence can be compensated, and however, this commonly requires precise knowledge about the probe antenna. In this work, the concept of NF far-field transformations (NFFFTs) with full correction of the influence of unknown probe antennas is introduced. Two nonconvex and two convex formulations are presented and their relation to the similar task of phase retrieval is highlighted. Simulation and measurement results illustrate the validity of the concept, shed light on the required complexity of measurement setups, and illustrate the limitations of the approach. Special attention is paid to the case of high practical relevance when AUT and probe are identical.**

***Index Terms*— Bilinear forms, inverse problem, near-field (NF) far-field (FF), nonconvex optimization, nonlinear, probe correction, unknown probe.**

I. Introduction

THE characterization of unknown antennas under test (AUTs) is commonly performed by sampling the radiated fields with precisely known probe antennas. In the case of near-field (NF) measurements, the fields caused by the radiator are sampled on an enclosing surface and the far-field (FF) characteristic is determined via an NF FF transformation (NFFFT). Dependent on the uniformity of the illumination of the AUT by the probe,[1] the radiation behavior of the probe antenna has more or less impact on the determination of the AUT radiation pattern. Typically, spherical measurement setups, where the probe is always facing the AUT under the same angle, need the least "amount" of probe correction, whereas accurate probe treatment is mandatory for planar or cylindrical measurements. The theory of probe correction [1], [2], [3], [4], [5], [6] in the context of antenna NF measurements [7] is well understood and has led to efficient transformation algorithms with full probe correction [8], [9], [10], [11], [12]. Considerable effort has been spent on comparing various probe compensations [13], e.g., no correction, first, second, or higher order [6], [14], [15] correction techniques. Further sources of error, such as inaccurate probe knowledge [16], positioning errors [17], the effect of cross-polarization [18], and the impact of general error sources in NF measurements [19], [20], have been investigated in depth.

There exists a manifold of special-purpose techniques, all of which feature distinct limitations, for the derivation of FF quantities of antennas from measurements in the NF with partially unknown probe antennas. Aiming at gain measurements, the two-antenna method [21], [22], originally defined for measurements in the FF and working with two unknown but identical antennas, has been developed and, later, extended to NF measurements [23, pp. 93–98] [24], [25]. However, and as pointed out in [5], it can neither be considered a rigorous, complete, nor reliable approach. Most information along the on-axis (main beam) direction of an antenna can be determined, where quadratic equations can only unambiguously be solved once prior information on the polarization of the AUT is given. Off-axis behavior in limited directions can be obtained once the AUT features additional symmetries. Still, experimental results for the on-axis gain determined from NF measurements neglecting cross-polar components have been reported in [26]. Similarly, the self-compensation approach introduced in [27] can be applied to determine the FF characteristic of an unknown AUT from NF measurements with an identical copy of itself, but only in cases where the AUT radiation behavior features symmetries. The three-antenna method [22], [28], [29], [30], based on three unknown antennas, can be employed to determine the absolute gain of antennas, however, requiring FF conditions and knowledge on polarization properties of the antennas. A generalization [31], [32] [23, pp. 98–102] with less restrictive measurement distances based on an extrapolation technique [33], [34] and requiring no a priori information on the polarizations has also been derived. Furthermore, utilizing NF correction terms valid for antennas with sinusoidal current distributions, the three-antenna method has been extended to the NF [35], [36]. Among the existing methods, solely the one briefly introduced by Hansen in [6, pp. 71–73], as an iterative scheme for probe calibration, relies on field transformation algorithms. Utilizing two sets of NF measurements, with the roles of AUT and probe interchanged, the probe and the AUT behaviors are iteratively and alternatingly determined, where convergence within a few iterations is reported for sufficiently simple probe models.

Manuscript received 11 November 2022; revised 15 March 2023; accepted 27 April 2023. Date of publication 19 May 2023; date of current version 7 July 2023. This work was supported in part by the German Federal Ministry for Economic Affairs and Climate Action (BMWK) under Grant 20E2124A. *(Corresponding author: Alexander Paulus.)*

The authors are with the Chair of High-Frequency Engineering, Department of Electrical Engineering, School of Computation, Information and Technology, Technical University of Munich, 80290 Munich, Germany (e-mail: a.paulus@tum.de).

Color versions of one or more figures in this article are available at https://doi.org/10.1109/TAP.2023.3276508.

Digital Object Identifier 10.1109/TAP.2023.3276508

[1]Due to reciprocity, illumination may be considered as a receiving or transmitting behavior.

We present and investigate four approaches for the realization of NFFFTs based on inverse-source models, which do not require the knowledge of the electromagnetic properties of the probe antenna, while they still fully compensate its influence. Instead of only determining the AUT representation, the transformations return the coefficients of AUT and probe equivalent sources. The resulting problem has a quadratic form and, among the existing approaches, it bears a slight similarity to the abovementioned NF two-antenna method introduced by Kerns [24]. Moreover, the iterative technique described by Hansen [6, pp. 71–73] is further investigated. Also, with its strong relation to the task of phaseless NFFFTs, the process requires a larger number of highly diverse measurement samples and a more careful implementation than for a conventional transformation with known probes. We start by reviewing the principle of inverse-source-based field transformations and its common mathematical representation with known probe antennas. Afterward, the probe itself is assumed to be unknown, which leads to a nonlinear problem statement. Solutions are presented in the form of a nonconvex and optimization-based method, a nonconvex approach that alternatingly determines the AUT and the probe unknowns, a convex and optimization-free approach emerging from the theory of bilinear forms, and a convex formulation utilizing semidefinite programming (SDP). The code for MATLAB [37] implementations of the convex optimization-free and the alternating algorithm is provided. Results obtained for complex-valued randomly distributed data verify the correctness of the approaches, while realistic simulation data of antenna NF measurements reveal natural limitations of transformations with unknown probes in general. Finally, results for a real-world measurement setup are presented. It is noted that parts of this work have been published in [38].

II. Field Transformation Algorithms

The principle of inverse-source-based NFFFTs is shown in Fig. 1. The main task is to determine the radiation pattern of an AUT from potentially truncated, irregularly arranged NF measurements with a probe antenna. The probe signals are collected in the measurement vector $\boldsymbol{b} \in \mathbb{C}^{m\times 1}$ and, in line with the uniqueness theorem [39], are expected to contain sufficient information in order to describe the electromagnetic radiation by the AUT. Furthermore, according to the equivalence principle [39], the AUT is represented by equivalent sources, e.g., in the form of electric $\boldsymbol{J}$ and magnetic $\boldsymbol{M}$ surface current densities, and these unknown coefficients are collected in the vector $\boldsymbol{z}_\mathrm{A} \in \mathbb{C}^{n_\mathrm{A}\times 1}$. Similarly, we assume that the probe antenna is modeled via the coefficients $\boldsymbol{z}_\mathrm{P} \in \mathbb{C}^{n_\mathrm{P}\times 1}$. The transformation itself can be considered a two-step process. Once the coefficients of the AUT have been determined from the NF samples, its radiation pattern within a valid angular region can be evaluated via the corresponding linear operator $\boldsymbol{A}_\mathrm{FF}$.

In this work, we differentiate between two particular cases of NF measurements and transformations. The most established scenario is that of known probe coefficients, where transformations with fully coherent [11], [40], [41], [42], [43] and incoherent [44], [45], [46], [47], [48], [49], [50], [51], [52], [53], [54], [55], [56], [57], [58] measurements exist. In particular, fully coherent measurements with a known probe antenna lead to an NFFFT, which essentially requires the solution of a linear system of equations. Nonlinearity is, for example, introduced if either measurements with incomplete phase information or with unknown probe antennas are performed—the latter is treated here. In case the probe coefficients are unknown, they must be determined in the course of the first part of the transformation—shown by the blue arrow in Fig. 1—, when the inverse problem is solved. It is crucial to realize that the loss of information with respect to fully coherent measurements, e.g., due to incoherence or unknown probe antennas, may render the uniqueness theorem inapplicable since a one-to-one relation between the measured fields and the probe signals is no longer a priori ensured.

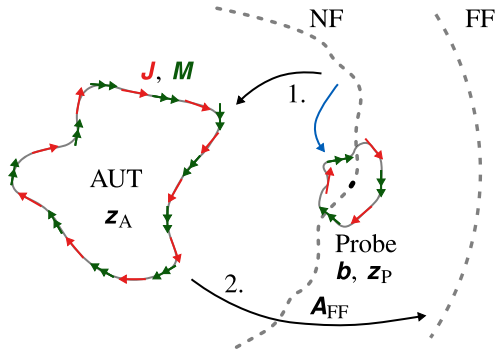

Fig. 1. Illustration of the NFFFT principle. The AUT NF is sampled by the probe, or its equivalent representation (here only drawn at one location), on the NF measurement surface. The AUT coefficients $\boldsymbol{z}_\mathrm{A}$ are determined from the measurements $\boldsymbol{b}$ via an inverse process. The FF of the AUT can then be evaluated via the operator $\boldsymbol{A}_\mathrm{FF}$. In case the probe coefficients $\boldsymbol{z}_\mathrm{P}$ are unknown, they have to be determined as part of the inverse problem.

Four approaches for the realization of NFFFTs with unknown probe antennas and full coherence are presented and discussed. For the purpose of clarification, the mathematical description of transformations with known probe antennas is reviewed first. The second part of the transformation, the computation of the FF, does not depend on the exact procedure of the first transformation step and, therefore, is not treated in more detail.

A. Transformation With Known Probes

A transformation for antenna NF measurements with known probe antennas leads to a linear system of equations

$$\boldsymbol{A}_\mathrm{NF}\,\boldsymbol{z}_\mathrm{A} = \boldsymbol{b}, \tag{1}$$

where the measurement matrix $\boldsymbol{A}_\mathrm{NF} \in \mathbb{C}^{m\times n_\mathrm{A}}$ incorporates the known probe behavior. As a result, the unknown AUT coefficients are linearly dependent on the complex-valued measurement vector. The first part of the transformation, as shown in Fig. 1, involves the solution of (1), which can be implemented efficiently and solved with existing, highly sophisticated NFFFTs, e.g., [40], [41]. When solving (1), e.g., by means of an iterative solver like the generalized minimal residual (GMRES) [59], least squares (LSQR) [60], or quasi-minimal residual (QMR) [61] method, one is most

often interested in minimizing the computational effort of the matrix–vector product, e.g., by applying an efficient approach such as the multilevel fast-multipole method [62], [63] or adaptive cross approximation [64] and reducing the required number of iterations via preconditioning [63], [65], [66], [67].

B. Transformation With Unknown Probes

If the probe coefficients $\boldsymbol{z}_\mathrm{P}$ are assumed to be unknown, they must be determined in addition to the AUT coefficients $\boldsymbol{z}_\mathrm{A}$. The procedure described here is motivated by the assumption that the probe coefficients correspond to spatial weights for field values generated by the AUT. However, the notation remains valid for different probe representations, e.g., in the spectral domain. For each measurement location $i \in \{1, \ldots, m\}$, a single row belonging to the forward operator $\boldsymbol{A}_\mathrm{NF}$ with probe correction will be expanded as n_P rows of an operator $\boldsymbol{A}_i \in \mathbb{C}^{n_\mathrm{P} \times n_\mathrm{A}}$ dependent on the probe basis functions. The row of $\boldsymbol{A}_\mathrm{NF}$ is obtained as the sum of the n_P rows of $\boldsymbol{A}_i$ weighted with the probe coefficients. Mathematically, we describe this via

$$\boldsymbol{z}_\mathrm{P}^\mathrm{T}\, \boldsymbol{A}_i\, \boldsymbol{z}_\mathrm{A} = \big[\boldsymbol{b}\big]_i \qquad \forall i \in \{1, \ldots, m\} \tag{2}$$

where the $[.]_i$ operator extracts the ith element of a vector. Since the probe coefficients are identical at each measurement location, i.e., a constant probe is assumed,[2] (2) does only vary in terms of the radiation operators $\boldsymbol{A}_i$ and the entries in the measurement vector. In total, the linear system in (1) has become a quadratic, thus a nonlinear system of equations depending on $(n_\mathrm{P} + n_\mathrm{A})$ unknowns. Therefore, assuming a nonredundant representation of the AUT and the probe, at least $m \geq (n_\mathrm{P} + n_\mathrm{A})$ measurements are expected to be required to determine the correct probe and AUT coefficients. In particular, nonredundant sets of unknowns are advisable for nonlinear problems, as they can both improve the convergence speed of nonlinear solvers and reduce the occurrence of suboptimal solutions. Interestingly, the problem of phaseless NFFFTs [44], [45], [46], [47], [48], [49], [50], [52], [53], [54], [57], [68], [69] can also be cast in the form of (2). In fact, the problem in (2) can be considered a generalization and, thus, more demanding version of the phase retrieval problem [70], [71], [72], [73], [74]. Due to this particular structure, at least four formulations can be employed to solve (2) and are presented in the following, where the nonconvex alternating iteration has already been introduced by Hansen [6, pp. 71–73].

Note that the introduced algorithms can be simplified to the case of an identical AUT and probe. This scenario might be of particular relevance in practice and, as is shown briefly in Section III, benefits from less impractical requirements regarding the measurement arrangement.

1) Nonconvex Simultaneous Implementation: One way of solving (2) is to cast it as an optimization problem of the form

$$\min_{\boldsymbol{z} \in \mathbb{C}^{n \times 1}} f(\boldsymbol{z}) = \|\mathcal{A}(\boldsymbol{z}) - \boldsymbol{b}\|_2^2 \tag{3}$$

with a stacked vector of unknowns $\boldsymbol{z} = [\boldsymbol{z}_\mathrm{P}^\mathrm{T}\ \boldsymbol{z}_\mathrm{A}^\mathrm{T}]^\mathrm{T} \in \mathbb{C}^{n \times 1}$ and an operator $\mathcal{A}: \mathbb{C}^{n \times 1} \rightarrow \mathbb{C}^{m \times 1}$ yet to be defined.

[2]The locations and orientations of the probe may still be arbitrary.

In this work, the minimization of (3) is performed via a first-order memory-limited Broyden–Fletcher–Goldfarb–Shanno (L-BFGS) method [75], [76], [77] employing an exact line search. For this specific implementation, the necessary Wirtinger derivative of [78], [79], [80], [81] (3) is found as

$$\frac{\partial f(\boldsymbol{z})}{\partial \boldsymbol{z}} = (\mathcal{A}(\boldsymbol{z}) - \boldsymbol{b})^\mathrm{H} \frac{\partial \mathcal{A}(\boldsymbol{z})}{\partial \boldsymbol{z}} + (\mathcal{A}(\boldsymbol{z}) - \boldsymbol{b})^\mathrm{T} \frac{\partial \overline{\mathcal{A}(\boldsymbol{z})}}{\partial \boldsymbol{z}}. \tag{4}$$

Since the cost function $f(\boldsymbol{z})$ is real-valued, no derivative with respect to the full conjugate coordinate is required.

Next, we stack all m equations of the form of (2) and define the operator

$$\mathcal{A}(\boldsymbol{z}) = \boldsymbol{C}\big(\boldsymbol{O}_1\boldsymbol{z} \circ \boldsymbol{O}_2\boldsymbol{z}\big) \tag{5}$$

with

$$\boldsymbol{O}_1\boldsymbol{z} = \big[\boldsymbol{z}_\mathrm{P}^\mathrm{T} \ \ldots\ \boldsymbol{z}_\mathrm{P}^\mathrm{T}\big]^\mathrm{T} \in \mathbb{C}^{n_\mathrm{P} m \times 1} \tag{6}$$

$$\boldsymbol{O}_2\boldsymbol{z} = \Big[\big[\boldsymbol{A}_1\boldsymbol{z}_\mathrm{A}\big]^\mathrm{T} \ \ldots\ \big[\boldsymbol{A}_m\boldsymbol{z}_\mathrm{A}\big]^\mathrm{T}\Big]^\mathrm{T} \in \mathbb{C}^{n_\mathrm{P} m \times 1}. \tag{7}$$

The elementwise multiplication of multidimensional variables is here denoted with "$\circ$". The matrix $\boldsymbol{O}_1$ extracts the probe coefficients from the stacked unknown vector $\boldsymbol{z}$ and duplicates them m times, whereas $\boldsymbol{O}_2$ extracts the AUT coefficients and applies them to all forward operators $\boldsymbol{A}_i$ dependent on the probe basis functions. The matrix $\boldsymbol{C} \in \mathbb{R}^{m \times n_\mathrm{P} m}$ is best described via its matrix–vector product

$$\boldsymbol{C}\boldsymbol{x} = \sum_{k=1}^{n_\mathrm{P}} \big[[\boldsymbol{x}]_k\ [\boldsymbol{x}]_{n_\mathrm{P}+k}\ \ldots\ [\boldsymbol{x}]_{(m-1)n_\mathrm{P}+k}\big]^\mathrm{T} \tag{8}$$

which extracts batches of n_P entries of an input vector $\boldsymbol{x} \in \mathbb{C}^{n_\mathrm{P} m \times 1}$ and adds them up. The procedure in (5) can be described as follows. The AUT sources are evaluated for all measurement locations and probe-dependent field data are generated via $\boldsymbol{O}_2\boldsymbol{z}$. These field values are then multiplied with the duplicated probe coefficients $\boldsymbol{O}_1\boldsymbol{z}$ and the summation of the "sub-probe signals" is done via the matrix $\boldsymbol{C}$.

For the operator defined via (5), the derivatives involved in (4) are found according to

$$\frac{\partial \mathcal{A}(\boldsymbol{z})}{\partial \boldsymbol{z}} = \boldsymbol{C}\big(\mathrm{diag}\big(\boldsymbol{O}_1\boldsymbol{z}\big)\boldsymbol{O}_2 + \mathrm{diag}\big(\boldsymbol{O}_2\boldsymbol{z}\big)\boldsymbol{O}_1\big) \tag{9}$$

whereas $(\partial\overline{\mathcal{A}(\boldsymbol{z})}/\partial\boldsymbol{z})$ equals a zero matrix and diag(.) creates a diagonal matrix from a vector.

As part of the iterative solver employed for the minimization of (3), the solution vector at the $(k+1)$th iteration is determined according to

$$\boldsymbol{z}_{k+1} = \boldsymbol{z}_k + \alpha_k \boldsymbol{p}_k \tag{10}$$

as a weighted sum of the solution of the previous iteration $\boldsymbol{z}_k$ and the descent direction $\boldsymbol{p}_k$, which is here determined via the L-BFGS method. The step length α_k is commonly numerically determined via a line search [77]. However, for the particular cost function and operator, a cubic equation for the optimal step length can be found. Inserting the solution at the next iteration into the cost function, one obtains the quartic polynomial

$$\begin{aligned} f\big(\boldsymbol{z}' = \boldsymbol{z} + \alpha\boldsymbol{p}\big) &= \big\|\boldsymbol{C}\big(\boldsymbol{O}_1\boldsymbol{z}' \circ \boldsymbol{O}_2\boldsymbol{z}'\big) - \boldsymbol{b}\big\|_2^2 \\ &= a\alpha^4 + b\alpha^3 + c\alpha^2 + d\alpha + e \end{aligned} \tag{11}$$

with

$$a = \left\| \boldsymbol{C}(\boldsymbol{O}_1\boldsymbol{p} \circ \boldsymbol{O}_2\boldsymbol{p}) \right\|_2^2 \tag{12}$$

$$b = 2\,\mathrm{Re}\Big\{ \big(\boldsymbol{C}(\boldsymbol{O}_1\boldsymbol{p} \circ \boldsymbol{O}_2\boldsymbol{z} + \boldsymbol{O}_2\boldsymbol{p} \circ \boldsymbol{O}_1\boldsymbol{z})\big)^{\mathrm{H}} \big(\boldsymbol{C}(\boldsymbol{O}_1\boldsymbol{p} \circ \boldsymbol{O}_2\boldsymbol{p})\big) \Big\} \tag{13}$$

$$c = \left\| \boldsymbol{C}(\boldsymbol{O}_1\boldsymbol{p} \circ \boldsymbol{O}_2\boldsymbol{z} + \boldsymbol{O}_2\boldsymbol{p} \circ \boldsymbol{O}_1\boldsymbol{z}) \right\|_2^2 + 2\,\mathrm{Re}\Big\{ \big(\boldsymbol{C}(\boldsymbol{O}_1\boldsymbol{z} \circ \boldsymbol{O}_2\boldsymbol{z}) - \boldsymbol{b}\big)^{\mathrm{H}} \big(\boldsymbol{C}(\boldsymbol{O}_1\boldsymbol{p} \circ \boldsymbol{O}_2\boldsymbol{p})\big) \Big\} \tag{14}$$

$$d = 2\,\mathrm{Re}\Big\{ \big(\boldsymbol{C}(\boldsymbol{O}_1\boldsymbol{z} \circ \boldsymbol{O}_2\boldsymbol{z}) - \boldsymbol{b}\big)^{\mathrm{H}} \big(\boldsymbol{C}(\boldsymbol{O}_1\boldsymbol{p} \circ \boldsymbol{O}_2\boldsymbol{z} + \boldsymbol{O}_2\boldsymbol{p} \circ \boldsymbol{O}_1\boldsymbol{z})\big) \Big\} \tag{15}$$

$$e = \left\| \boldsymbol{C}(\boldsymbol{O}_1\boldsymbol{z} \circ \boldsymbol{O}_2\boldsymbol{z}) - \boldsymbol{b} \right\|_2^2. \tag{16}$$

The first-order necessary condition for a stationary point requires the derivative of (11) to be zero, i.e.,

$$\frac{\partial f(\boldsymbol{z}')}{\partial \alpha} = 4a\alpha^3 + 3b\alpha^2 + 2c\alpha + d \stackrel{!}{=} 0. \tag{17}$$

The zeros of a cubic polynomial can be found analytically, e.g., see [82, pp. 179–180]. Since the cost function was here shown to be representable as a quartic polynomial, the minimization of (3) for the task of an NFFFT with unknown probe antennas is nonlinear and nonconvex. The occurrence of local stationary points is thus expected to potentially prohibit finding the globally optimal solution. In fact, one can show that the problem becomes convex if

$$\frac{b^2}{ac'} < \frac{32}{9} \qquad \forall \boldsymbol{p} \in \mathbb{C}^{n\times 1} \tag{18}$$

with

$$c' = \left\| \boldsymbol{C}(\boldsymbol{O}_1\boldsymbol{p} \circ \boldsymbol{O}_2\boldsymbol{z} + \boldsymbol{O}_2\boldsymbol{p} \circ \boldsymbol{O}_1\boldsymbol{z}) \right\|_2^2. \tag{19}$$

The derivation of (18) is analogous to that for the convexity analysis of the phase retrieval problem [83], of which the geometry, stationary points, and uniqueness have been a topic of intense research [74], [84], [85], [86], [87], [88], [89], [90], [91], [92]. First, one starts at the correct solution $\boldsymbol{z}$, i.e., $\boldsymbol{C}(\boldsymbol{O}_1\boldsymbol{z} \circ \boldsymbol{O}_2\boldsymbol{z}) - \boldsymbol{b} = \boldsymbol{0}$, and determines the nonzero roots of the derivative in (17), which are found from a polynomial of second order. As soon as the condition in (18) is fulfilled (for all search directions), no real-valued, nonzero roots are found for the polynomial, meaning that the cost function exhibits its sole global minimum at the correct solution and, thus, is convex.

2) Convex, Simultaneous Implementation: A convex approach to (2) can be found via the theory of bilinear forms [93], [94], [95], which has also been applied to incoherent NFFFTs [96]. Motivation can be drawn from considering a modified version of (2) in the form of

$$\boldsymbol{z}_{\mathrm{P}}^{\mathrm{T}} \boldsymbol{P}_{ij} \boldsymbol{z}_{\mathrm{A}} = [\boldsymbol{z}_{\mathrm{P}}]_i [\boldsymbol{z}_{\mathrm{A}}]_j = \big[\tilde{\boldsymbol{b}}\big]_k \tag{20}$$

which involves a desired measurement entry $[\tilde{\boldsymbol{b}}]_k$ and the corresponding measurement matrix $\boldsymbol{P}_{ij}$. The latter only contains a single nonzero unit entry in the ith row and the jth column. A particular set of measurements $\tilde{\boldsymbol{b}}$ belonging to a certain set of $\boldsymbol{P}_{ij}$ (for various i and j) can then be employed to easily reconstruct $\boldsymbol{z}_{\mathrm{P}}$ and $\boldsymbol{z}_{\mathrm{A}}$ up to global scaling.[3] The issue is that the $[\tilde{\boldsymbol{b}}]_k$ belonging to the required forward matrices $\boldsymbol{P}_{ij}$ may not have been acquired during the NF measurement, instead only the $\boldsymbol{A}_i$ and $[\boldsymbol{b}]_i$ are available. However, due to linearity of (2) with respect to the $\boldsymbol{A}_i$ we can determine the coefficients $\boldsymbol{z}_k \in \mathbb{C}^{m\times 1}$ such that

$$\boldsymbol{P}_{ij} = \sum_{l=1}^{m} [\boldsymbol{z}_k]_l \boldsymbol{A}_l. \tag{21}$$

Once the $\boldsymbol{z}_k$ have been found, the kth measurement entry belonging to the matrix $\boldsymbol{P}_{ij}$

$$\big[\tilde{\boldsymbol{b}}\big]_k = \sum_{l=1}^{m} [\boldsymbol{z}_k]_l \big[\boldsymbol{b}\big]_l \tag{22}$$

can be evaluated. The remaining main effort is to find a procedure for the computation of the $\boldsymbol{z}_k$.

Starting from (20), one can determine a normal system of equations of the form

$$\boldsymbol{Q}^{\mathrm{H}} \boldsymbol{Q} \boldsymbol{z}_k = \boldsymbol{Q}^{\mathrm{H}} \boldsymbol{p}_{ij} \tag{23}$$

with $\boldsymbol{Q} \in \mathbb{C}^{n_{\mathrm{P}} n_{\mathrm{A}} \times m}$ and $\boldsymbol{p}_{ij} \in \mathbb{C}^{n_{\mathrm{P}} n_{\mathrm{A}} \times 1}$. The lth column of $\boldsymbol{Q}$ contains all columns of the measurement matrix $\boldsymbol{A}_l$ stacked into a single vector. Similarly, the vector $\boldsymbol{p}_{ij}$ corresponds to the stacking of all columns of the matrix $\boldsymbol{P}_{ij}$. However, (23) can be rewritten as

$$\begin{bmatrix} \mathrm{Tr}(\boldsymbol{A}_1^{\mathrm{H}}\boldsymbol{A}_1) & \dots & \mathrm{Tr}(\boldsymbol{A}_1^{\mathrm{H}}\boldsymbol{A}_m) \\ \vdots & \ddots & \vdots \\ \mathrm{Tr}(\boldsymbol{A}_m^{\mathrm{H}}\boldsymbol{A}_1) & \dots & \mathrm{Tr}(\boldsymbol{A}_m^{\mathrm{H}}\boldsymbol{A}_m) \end{bmatrix} \boldsymbol{z}_k = \begin{bmatrix} \mathrm{Tr}(\boldsymbol{A}_1^{\mathrm{H}}\boldsymbol{P}_{ij}) \\ \vdots \\ \mathrm{Tr}(\boldsymbol{A}_m^{\mathrm{H}}\boldsymbol{P}_{ij}) \end{bmatrix} \tag{24}$$

where Tr(.) returns the trace of a matrix. Note that (24) only returns meaningful results if the original system $\boldsymbol{Q}\boldsymbol{z}_k = \boldsymbol{p}_{ij}$ has full rank, which requires[4] $m \geq n_{\mathrm{P}} n_{\mathrm{A}}$.

Let us summarize the convex solution approach to the NFFFT with unknown probe coefficients exploiting bilinear forms. First, define a set of matrices $\boldsymbol{P}_{ij}$, such that the corresponding measurements in $\tilde{\boldsymbol{b}}$ allow for a reconstruction of $\boldsymbol{z}_{\mathrm{P}}$ and $\boldsymbol{z}_{\mathrm{A}}$. Second, insert these matrices into (24) and compute the corresponding vectors $\boldsymbol{z}_k$. Third, entrywise multiply $\boldsymbol{b}$ with $\boldsymbol{z}_k$ and sum the result in order to obtain the elements $[\tilde{\boldsymbol{b}}]_k$. In the last step, evaluate $\boldsymbol{z}_{\mathrm{P}}$ and $\boldsymbol{z}_{\mathrm{A}}$ from the $[\tilde{\boldsymbol{b}}]_k$.

For the purpose of illustration, consider the case of $n_{\mathrm{P}} = 2$ and $n_{\mathrm{A}} = 3$. According to the first step, a simple choice for the matrices $\boldsymbol{P}_{ij}$ is

$$\boldsymbol{z}_{\mathrm{P}}^{\mathrm{T}} \boldsymbol{P}_{11} \boldsymbol{z}_{\mathrm{A}} = \boldsymbol{z}_{\mathrm{P}}^{\mathrm{T}} \begin{bmatrix} 1 & 0 & 0 \\ 0 & 0 & 0 \end{bmatrix} \boldsymbol{z}_{\mathrm{A}} = [\boldsymbol{z}_{\mathrm{P}}]_1 [\boldsymbol{z}_{\mathrm{A}}]_1 = \big[\tilde{\boldsymbol{b}}\big]_1 \tag{25}$$

$$\boldsymbol{z}_{\mathrm{P}}^{\mathrm{T}} \boldsymbol{P}_{12} \boldsymbol{z}_{\mathrm{A}} = \boldsymbol{z}_{\mathrm{P}}^{\mathrm{T}} \begin{bmatrix} 0 & 1 & 0 \\ 0 & 0 & 0 \end{bmatrix} \boldsymbol{z}_{\mathrm{A}} = [\boldsymbol{z}_{\mathrm{P}}]_1 [\boldsymbol{z}_{\mathrm{A}}]_2 = \big[\tilde{\boldsymbol{b}}\big]_2 \tag{26}$$

$$\boldsymbol{z}_{\mathrm{P}}^{\mathrm{T}} \boldsymbol{P}_{13} \boldsymbol{z}_{\mathrm{A}} = \boldsymbol{z}_{\mathrm{P}}^{\mathrm{T}} \begin{bmatrix} 0 & 0 & 1 \\ 0 & 0 & 0 \end{bmatrix} \boldsymbol{z}_{\mathrm{A}} = [\boldsymbol{z}_{\mathrm{P}}]_1 [\boldsymbol{z}_{\mathrm{A}}]_3 = \big[\tilde{\boldsymbol{b}}\big]_3 \tag{27}$$

$$\boldsymbol{z}_{\mathrm{P}}^{\mathrm{T}} \boldsymbol{P}_{21} \boldsymbol{z}_{\mathrm{A}} = \boldsymbol{z}_{\mathrm{P}}^{\mathrm{T}} \begin{bmatrix} 0 & 0 & 0 \\ 1 & 0 & 0 \end{bmatrix} \boldsymbol{z}_{\mathrm{A}} = [\boldsymbol{z}_{\mathrm{P}}]_2 [\boldsymbol{z}_{\mathrm{A}}]_1 = \big[\tilde{\boldsymbol{b}}\big]_4. \tag{28}$$

[3] Any pair of solution vectors $\boldsymbol{z}'_{\mathrm{P}} = s\,\boldsymbol{z}_{\mathrm{P}}$ and $\boldsymbol{z}'_{\mathrm{A}} = (1/s)\,\boldsymbol{z}_{\mathrm{A}}$ with a nonzero scaling $s \in \mathbb{C}$ fulfills (2).

[4] Again, assuming a nonredundant representation of AUT and probe.

Second, the $\boldsymbol{P}_{ij}$ matrices from (25) to (28) are inserted into (24) leading to $\boldsymbol{z}_k$ for $k \in \{1, \ldots, (n_\mathrm{A}-1)n_\mathrm{P}\}$ at the expense of solving $(n_\mathrm{A}-1)n_\mathrm{P}$ linear systems of equations. Third, we compute $\mathbb{C} \ni [\tilde{\boldsymbol{b}}]_k = \boldsymbol{b}^\mathrm{T}\boldsymbol{z}_k \ \forall k$. Fourth, since the pair of AUT and probe coefficients can only be determined up to global scaling, we arbitrarily set $[\boldsymbol{z}_\mathrm{A}]_1 = 1$ and determine the remaining unknowns as

$$[\boldsymbol{z}_\mathrm{P}]_1[\boldsymbol{z}_\mathrm{A}]_1 = [\boldsymbol{z}_\mathrm{P}]_1 = \big[\tilde{\boldsymbol{b}}\big]_1, \quad [\boldsymbol{z}_\mathrm{A}]_2 = \big[\tilde{\boldsymbol{b}}\big]_2 / \big[\tilde{\boldsymbol{b}}\big]_1 \tag{29}$$

$$[\boldsymbol{z}_\mathrm{P}]_2[\boldsymbol{z}_\mathrm{A}]_1 = [\boldsymbol{z}_\mathrm{P}]_2 = \big[\tilde{\boldsymbol{b}}\big]_4, \quad [\boldsymbol{z}_\mathrm{A}]_3 = \big[\tilde{\boldsymbol{b}}\big]_3 / \big[\tilde{\boldsymbol{b}}\big]_1. \tag{30}$$

In case the first entry of the AUT coefficients is zero, the same principle can be applied by setting a different AUT coefficient to unity and solving for the remaining quantities.

The complete procedure valid for arbitrary dimensions is given in Algorithm 1 in MATLAB [37] notation. The trace operation is here more efficiently evaluated by summing all entries of the elementwise multiplication of the involved matrices. From a computational perspective, the construction of the normal system of equations in (23) features the computational complexity of $\mathcal{O}(m^2 n_\mathrm{P} n_\mathrm{A})$. Since $m \geq n_\mathrm{P} n_\mathrm{A}$ is required for the approach to return meaningful results, the construction of $\boldsymbol{Q}^\mathrm{H}\boldsymbol{Q}$ and, thus, the overall computational complexity of the convex transformation based on bilinear forms scale according to $\mathcal{O}((n_\mathrm{P} n_\mathrm{A})^3)$.

3) Nonconvex Alternating Implementation: As motivated by Hansen [6, pp. 71–73], instead of simultaneously determining the probe and the AUT coefficients, one can sequentially compute one of both quantities while keeping the other fixed. Due to the linear dependency of both sets of coefficients on the measurement vector, this results in an alternating solution of linear systems of equations. For example, starting with an initial guess for the probe coefficients $\boldsymbol{z}_{\mathrm{P}0}$, one can determine the AUT unknowns via

$$\boldsymbol{z}_\mathrm{A} = \boldsymbol{M}^\dagger \boldsymbol{b} \tag{31}$$

with a matrix $\boldsymbol{M} \in \mathbb{C}^{m \times n_\mathrm{A}}$ dependent on $\boldsymbol{z}_{\mathrm{P}0}$ and constructable with Algorithm 2. Here, the Moore–Penrose inverse is denoted by $\boldsymbol{M}^\dagger$. Afterward, a new guess for the probe coefficients is obtained from

$$\boldsymbol{z}_\mathrm{P} = \boldsymbol{N}^\dagger \boldsymbol{b} \tag{32}$$

where the computation of $\boldsymbol{N} \in \mathbb{C}^{m \times n_\mathrm{P}}$ from a given $\boldsymbol{z}_\mathrm{A}$ is described in Algorithm 3. The MATLAB implementation referring to Algorithms 2 and 3 is shown in Algorithm 4.

4) Convex Implementation via Semidefinite Programming With Identical AUT and Probe: For the case when the AUT and the probe are both unknown, but identical, (2) simplifies to

$$\boldsymbol{z}^{\star\mathrm{T}}\boldsymbol{A}_i\boldsymbol{z}^\star = \big[\boldsymbol{b}\big]_i \qquad \forall i \in \{1, \ldots, m\} \tag{33}$$

with $\boldsymbol{z}^\star \in \mathbb{C}^{n^\star \times 1}$ and $n^\star = n_\mathrm{A} = n_\mathrm{P}$. Note that the presented approaches for solving (2) can easily be adapted to exploit $\boldsymbol{z}_\mathrm{A} = \boldsymbol{z}_\mathrm{P}$ and thus solve (33). Details are provided in Section III-B3. Here, an alternative approach for solving (33), which relies on SDP [97], [98] is derived. The procedure follows ideas in [99], intended for the case of phase retrieval, to arrive at a description in terms of real-valued quantities. We start by stacking the real and imaginary parts of the unknown coefficients as

$$\tilde{\boldsymbol{z}} = \big[\mathrm{Re}\{\boldsymbol{z}^\star\}^\mathrm{T} \ \mathrm{Im}\{\boldsymbol{z}^\star\}^\mathrm{T}\big]^\mathrm{T}. \tag{34}$$

Similar, the operators

$$\boldsymbol{A}_i' = \begin{bmatrix} \mathrm{Re}\{\boldsymbol{A}_i\} & -\mathrm{Im}\{\boldsymbol{A}_i\} \\ -\mathrm{Im}\{\boldsymbol{A}_i\} & -\mathrm{Re}\{\boldsymbol{A}_i\} \end{bmatrix} \tag{35}$$

$$\boldsymbol{A}_i'' = \begin{bmatrix} \mathrm{Im}\{\boldsymbol{A}_i\} & \mathrm{Re}\{\boldsymbol{A}_i\} \\ \mathrm{Re}\{\boldsymbol{A}_i\} & -\mathrm{Im}\{\boldsymbol{A}_i\} \end{bmatrix} \tag{36}$$

are defined such that (2) can be written as

$$\begin{aligned} \tilde{\boldsymbol{z}}^\mathrm{T}\boldsymbol{A}_i'\tilde{\boldsymbol{z}} &= \mathrm{Re}\big\{\big[\boldsymbol{b}\big]_i\big\} \\ \tilde{\boldsymbol{z}}^\mathrm{T}\boldsymbol{A}_i''\tilde{\boldsymbol{z}} &= \mathrm{Im}\big\{\big[\boldsymbol{b}\big]_i\big\}. \end{aligned} \qquad \forall i \in \{1, \ldots, m\}. \tag{37}$$

We can then define the real-valued, positive-semidefinite rank-one matrix $\boldsymbol{Z}' = \tilde{\boldsymbol{z}}\tilde{\boldsymbol{z}}^\mathrm{T} \in \mathbb{R}^{2n^\star \times 2n^\star}$, for which we find

$$\tilde{\boldsymbol{z}}^\mathrm{T}\boldsymbol{A}_i'\tilde{\boldsymbol{z}} = \mathrm{Tr}\big(\boldsymbol{Z}'\boldsymbol{A}_i'\big). \tag{38}$$

The nonconvexity of the rank constraint can be avoided by employing a convex proxy in the form of the minimization of the trace of $\boldsymbol{Z}'$. Finally, we formulate the task of an NFFFT with unknown probe, when AUT and probe are identical, as the convex SDP task

$$\begin{aligned} \min_{\boldsymbol{Z}' \in \mathbb{R}^{2n^\star \times 2n^\star}} \quad & \mathrm{Tr}\big(\boldsymbol{Z}'\big) \\ \text{s.t.} \quad & \mathrm{Tr}\big(\boldsymbol{Z}'\boldsymbol{A}_i'\big) = \mathrm{Re}\big\{\big[\boldsymbol{b}\big]_i\big\} \\ & \mathrm{Tr}\big(\boldsymbol{Z}'\boldsymbol{A}_i''\big) = \mathrm{Im}\big\{\big[\boldsymbol{b}\big]_i\big\} \\ & \boldsymbol{Z}' \succeq 0 \end{aligned} \qquad \forall i \in \{1, \ldots, m\}. \tag{39}$$

As commonly encountered in SDP and as has been seen with the linear approach directly exploiting the properties of bilinear forms in Section II-B2, the number of unknowns is lifted and, thus, effectively squared. The applicability of (39) may thus be limited to small-sized problems. For completeness, it should be mentioned that the SDP formulation could also be adapted to the asymmetric case when the AUT and the probe are not identical, e.g., by means of zero padding in order to arrive at square matrices required for the application of the trace operation. For the sake of brevity, this has not been further considered in this work.

III. Numerical Results and Discussion

As a proof of concept, the presented methods are first verified with complex-valued normally distributed operators $\boldsymbol{A}_i$ and solution vectors $\boldsymbol{z}_\mathrm{P}$ and $\boldsymbol{z}_\mathrm{A}$. Afterward, simulated antenna NF data are employed. Furthermore, the case of identical AUT and probe is investigated, for which the SDP-based formulation in (39) is briefly tested and the other formulations are adapted. Finally, measurement data of two identical horn antennas at 40 GHz are considered.

A. Random Data

Consider a toy example with $n_\mathrm{P} = 3$ and $n_\mathrm{A} = 6$ for randomly distributed $\boldsymbol{A}_i$, $i \in \{1, \ldots, m\}$. No precautions are taken to avoid inverse crime. Figure 2 shows the achievable success rate of three of the formulations when varying the ratio

Algorithm 1 Convex AUT and Probe Reconstruction via Bilinear Forms (MATLAB Code)

Input: cell array `Ai` $= \boldsymbol{A}_i$, vector `b` $= \boldsymbol{b}$
Output: vectors of coefficients `zp` $= \boldsymbol{z}_\mathrm{P}$ and `za` $= \boldsymbol{z}_\mathrm{A}$

```
% Number of measurements :
m = numel(b);
% Number of probe coefficients :
np = size(Ai{1},1);
% Number of AUT coefficients :
na = size(Ai{1},2);
% Construct Q^H Q matrix :
QHQ = NaN(m,m);
for d = 1:m
    for e = d:m
        t = conj(Ai{d}).*Ai{e};
        QHQ(d,e) = sum(t(:));
        QHQ(e,d) = conj(QHQ(d,e));
    end
end
% Construct P_ij matrices :
Pij = cell(np+na-1,1);
for d = 1:na
    Pij{d,1} = zeros(np,na);
    Pij{d,1}(1,d) = 1;
end
for d = na+1:np+na-1
    Pij{d,1} = zeros(np,na);
    Pij{d,1}(d-na+1,1) = 1;
end
% Construct Q^H p_ij vectors :
QHpij = NaN(m,np+na-1);
for d = 1:np+na-1
    for e = 1:m
        t = conj(Ai{e,1}).*Pij{d,1};
        QHpij(e,d) = sum(t(:));
    end
% Solve (n_A - 1)n_P linear systems :
zk = QHQ\QHpij;
% Determine b~ :
btilde = sum(zk.*b,1);
% Evaluate z_P and z_A :
za(1,1) = 1;
zp(1,1) = btilde(1);
za(2:na,1) = btilde(2:na)/zp(1,1);
zp(2:np,1) = btilde(na+1:na+np-1).';
return zp, za
```

Algorithm 2 Construct Measurement Matrix for AUT Coefficients (MATLAB Code)

Input: cell array `Ai` $= \boldsymbol{A}_i$, probe coefficients `zp` $= \boldsymbol{z}_\mathrm{P}$
Output: matrix `M` $= \boldsymbol{M}$

```
m = numel(Ai);
na = size(Ai{1},2);
M = NaN(mi,na);
for a = 1:m
    M(a,:) = (Ai{a}.'*zp(:)).';
end
return M
```

Algorithm 3 Construct Measurement Matrix for Probe Coefficients (MATLAB Code)

Input: cell array `Ai` $= \boldsymbol{A}_i$, AUT coefficients `za` $= \boldsymbol{z}_\mathrm{A}$
Output: matrix `N` $= \boldsymbol{N}$

```
m = numel(Ai);
np = size(Ai{1},1);
N = NaN(m,np);
for a = 1:m
    N(a,:) = Ai{a}*za(:);
end
return N
```

of measurements $m \in \{3, \ldots, 30\}$ with respect to the product $n_\mathrm{P} n_\mathrm{A} = 18$. Success is declared once a relative deviation

$$\epsilon_\mathrm{dB}(\boldsymbol{z}, \hat{\boldsymbol{z}}) = 20 \log \left(\frac{\|\boldsymbol{z} - \hat{\boldsymbol{z}}\|_2}{\|\boldsymbol{z}\|_2} \right) \tag{40}$$

for the reconstructed probe $\hat{\boldsymbol{z}}_\mathrm{P}$ and the AUT coefficients $\hat{\boldsymbol{z}}_\mathrm{A}$ with respect to the true coefficients of below -60 dB is achieved. The nonconvex solvers at most performed 5×10^2 iterations and started from a random initial guess. At each ratio

Algorithm 4 Alternating Probe and AUT Reconstruction (MATLAB Pseudocode)

Input: cell array `Ai` $= \boldsymbol{A}_i$, measurement vector `b` $= \boldsymbol{b}$, initial guess `zp0` $= \boldsymbol{z}_{\mathrm{P}0}$, iterations `k` $= k_\mathrm{it}$
Output: vectors of coefficients `zp` $= \boldsymbol{z}_\mathrm{P}$ and `za` $= \boldsymbol{z}_\mathrm{A}$

```
zp = zp0;
for a = 1:k
    M ← Alg. 2 from zp
    za = M\b(:);
    N ← Alg. 3 from za
    zp = N\b(:);
end
return zp, za
```

of $m/(n_\mathrm{P} n_\mathrm{A})$, in total, 10^3 repetitions with randomly drawn operators and solution vectors were considered. As expected, the convex approach returns the correct solutions once $m \geq n_\mathrm{P} n_\mathrm{A}$. In contrast, the nonconvex approaches may provide an accurate solution for far fewer measurement samples. However, they may get stuck at suboptimal solutions even for large m—in Fig. 2, and the nonconvex techniques achieve success rates close to 100 %, but fail in some cases. Overall, all three techniques remain stable and provide consistent results when redundant samples are added, i.e., $m > (n_\mathrm{P} n_\mathrm{A})$. Starting from a random initial guess, the nonconvex methods even sometimes converge to the true solution when the problem is underdetermined, i.e., $m < (n_\mathrm{P} + n_\mathrm{A})$ or, in Fig. 2, $m/(n_\mathrm{P} n_\mathrm{A}) < 0.5$, resulting in a nonzero success rate. In general, however, and for larger problems, there is only a realistic chance of finding an accurate solution if the number of measurements exceeds or equals the sum of the degrees of freedom of the AUT and the probe.

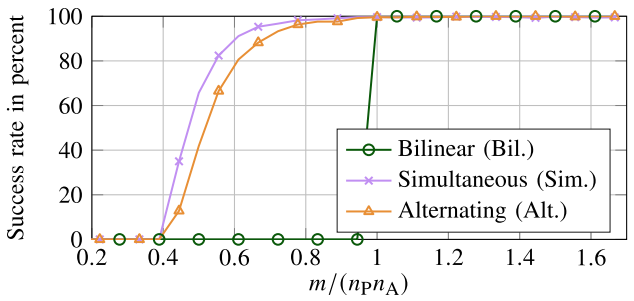

Fig. 2. Probe and AUT reconstruction for $n_\mathrm{P} = 3$ and $n_\mathrm{A} = 6$ with randomly distributed data.

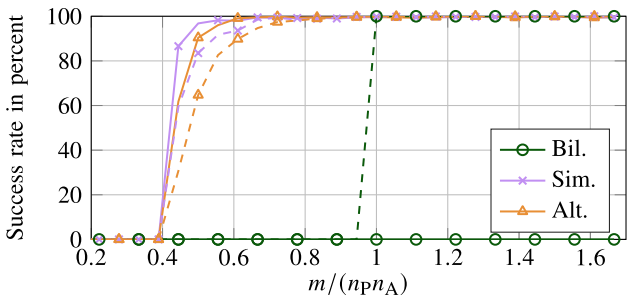

Fig. 3. Probe and AUT reconstruction for $n_\mathrm{P} = 3$ and $n_\mathrm{A} = 6$ with spherical NF data. Probe pointing toward the AUT (solid) and randomly oriented probe (dashed).

B. Simulated Antenna NF Data

1) Spherical Setup: In a first investigation, similar simulations as done with the random data model are conducted with NF operators belonging to a spherical measurement setup. Again, no precautions are taken to avoid inverse crime. It is noteworthy to highlight the difference between the AUT and the probe in this particular measurement configuration. From the perspective of the AUT, the probe is moving and thus illuminating different parts of the AUT during the measurement. From the perspective of the probe, the AUT is revolving around itself while staying at the same location relative to the probe at all times. Therefore, mostly, the radiation characteristic of the probe toward its front direction is relevant and sampled by the AUT. Consequently, for this setup, the task of determining the AUT coefficients is most likely better posed than that of finding the probe representation. In the example considered here, the AUT is represented by six randomly excited spherical vector wave functions [6] and its field is sampled by a probe consisting of three Hertzian dipoles. Figure 3 shows the success rate of the nonconvex methods and the bilinear algorithm for two cases. First, a classical probe arrangement is assumed, where the probe is always directed toward the AUT. In a second scenario, for which the results are drawn with dashed lines in Fig. 3, the orientation of the probe was randomly chosen at each measurement location. This can be seen as an attempt to align the roles of AUT and probe since now the relative motion of AUT to probe, and vice versa, is similar. The solver settings and repetitions were identical to those of Fig. 2. While the nonconvex solvers are able to determine the AUT and the probe coefficients in both scenarios correctly, the convex bilinear solver fails for the classical spherical setup. Evidently, $m \geq n_\mathrm{P}n_\mathrm{A}$ is a necessary but not sufficient condition for the solver to succeed. Whenever the measurement matrices $\boldsymbol{A}_i$ exhibit strong similarities to each other, they may not represent a complete basis required for the construction of the matrices $\boldsymbol{P}_{ij}$. In practice, this happens for insufficient variations of the probe illumination, which is inherent to classical spherical measurement setups. Similar to the discussion of Fig. 2, the nonzero success rates for $m < (n_\mathrm{P} + n_\mathrm{A})$, i.e., $m/(n_\mathrm{P}n_\mathrm{A}) < 0.5$, in Fig. 3 should be interpreted with care, as they are less likely to be observed for larger problems and when the inverse crime problem is prevented.

2) Planar Setup: Next, a synthetic planar antenna NF measurement setup is considered. The true AUT is given in the form of equivalent Hertzian dipoles on a sphere with a radius of λ. The coefficients of the AUT dipoles are generated by backpropagating a z-polarized plane wave coming from the $+x$-direction. In order to avoid inverse crime, the reconstruction of the AUT is done in terms of 336 spherical vector wave functions. As shown in Fig. 4(a), the distance between the equivalent sphere of the AUT and the square acquisition plane with a side length of 12λ is 3λ. The probe antenna, shown in Fig. 4(b), is modeled as a 1-D broadside array with a length of 2λ (along the y'-axis in the probe coordinate system) and consisting of ten Hertzian dipoles in total, five dipoles oriented in the vertical z'-direction and five in the horizontal y'-direction. The probe coefficients are set by backpropagating a z'-polarized plane wave coming from the $+x'$-direction, which is, however, rotated around the $\mathcal{X}'$-axis by 2° and around the φ'-axis by $-1°$—causing a tilted main beam and a nonnegligible cross-polar component. The tilted behavior of this "true" probe is supposed to represent a potential misalignment when placing the probe antenna on a mounting structure in a real-world measurement setup. In contrast, assuming a perfectly aligned probe, the pattern denoted with "assumed" is obtained, which corresponds to probe coefficients of unity and zero for co-polar and cross-polar dipoles, respectively. If no probe correction at all is applied, the probe is identical to a z'-oriented Hertzian dipole.

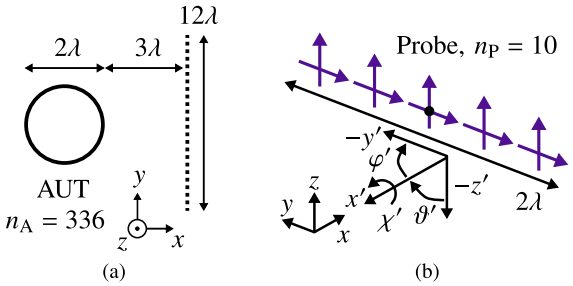

Fig. 4. (a) Synthetic measurement setup. (b) Probe array (purple arrows) centered in the probe origin (black dot) with orientation defined via angles $(\vartheta', \varphi', \mathcal{X}')$, drawn for $(\vartheta' = 90°, \varphi' = 0°, \mathcal{X}' = 0°)$.

The purpose of the following study is to investigate the effect of a false probe correction, i.e., correcting with the assumed probe or without any probe correction, and the potential accuracy benefits associated with the proposed transformations without requiring knowledge of the probe radiation pattern or coefficients. Therefore, six transformation

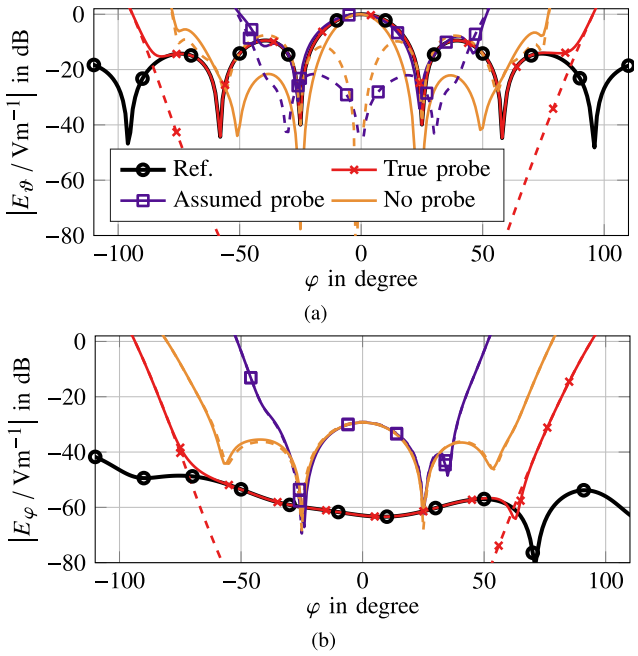

Fig. 5. AUT FF pattern for $\vartheta = 90°$ computed from planar NF measurements with two probe orientations $\mathcal{X}' \in \{0°, 90°\}$. Probe correction with the true probe behavior (tilted), the assumed (nontilted) behavior, and no probe correction at all. (a) Co-polar fields. (b) Cross-polar fields. Dashed lines represent $\epsilon_{\mathrm{dB,FF}}$.

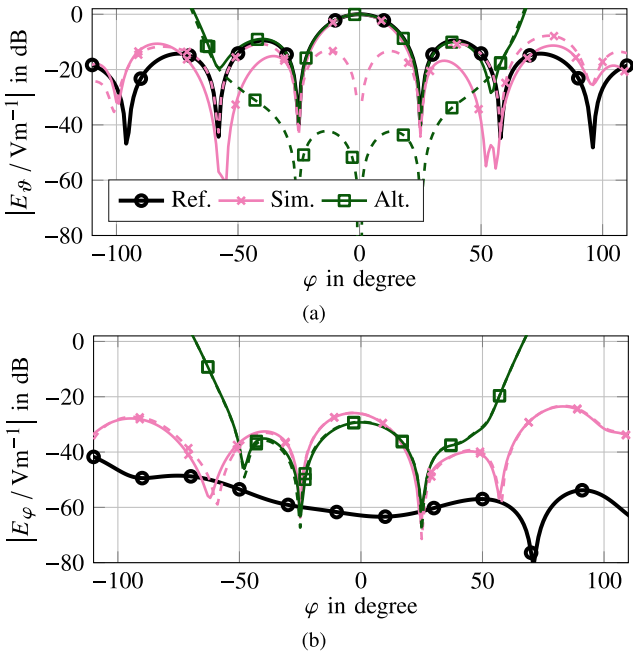

Fig. 6. AUT FF pattern for $\vartheta = 90°$ computed from planar NF measurements with two probe orientations $\mathcal{X}' \in \{0°, 90°\}$. Results for unknown probe coefficients employing the nonconvex simultaneous optimization-based approach and the nonconvex alternating technique. (a) Co-polar fields. (b) Cross-polar fields. Dashed lines represent $\epsilon_{\mathrm{dB,FF}}$.

procedures are applied to three different measurement scenarios. In all three scenarios, the NF of the AUT is sampled by the true, i.e., tilted and rotated, probe antenna, and the differences between the three scenarios are based on the number of sampling points on the measurement plane, as well as the orientation angles of the probe at the measurement locations. Furthermore, the probe coordinate system is always chosen such that the probe's x'-axis is pointing in the $-x$-direction in the AUT coordinate system [see Fig. 4(b)]. First, and as a reference, we consider a transformation knowing and employing the true probe as part of a probe correction. Second, a transformation applying a probe correction with the assumed, i.e., not tilted, probe is performed. Third, the NF is transformed without probe correction. Fourth, fifth, and sixth employ the simultaneous nonconvex, the alternating nonconvex, and the convex bilinear transformation where the probe is modeled by the identical ten dipoles of the true probe, respectively, however, without knowledge of the correct coefficients. While this corresponds to inverse crime in terms of the probe, the procedure allows to keep the overall number of unknowns within a reasonable range, which is particularly important for the convex algorithm to remain applicable.

Note that the orientation of the probe array in Fig. 4(b) is uniquely defined via the three angles $(\vartheta', \varphi', \mathcal{X}')$, where $(\vartheta' = 90°, \varphi' = 0°, \mathcal{X}' = 0°)$ corresponds to a main beam (approximately) pointing along the $+x'$-direction with a co-polarization along the z'-axis.

a) Probe rotation around x': At each of 625 sample locations on the measurement plane, the AUT fields were acquired for two polarization angles of the probe oriented perpendicular to the measurement plane, i.e., as done in a typical planar NF measurement and corresponding to $(\vartheta' = 90°, \varphi' = 0°, \mathcal{X}' \in \{0°, 90°\})$. By rotating the probe around $\mathcal{X}'$, the cross- and the co-polar fields of the AUT are measured, leading to a total of $m = 1250$ probe signals.

The results of the three transformation approaches based on a known probe are shown in Fig. 5. The reconstructed FF of the AUT in the plane of $\vartheta = 90°$ is drawn and the relative magnitude FF deviation

$$\epsilon_{\mathrm{dB,FF}}(\boldsymbol{E}_{\mathrm{ref}}, \boldsymbol{E}_{\mathrm{rec}}) = 20 \log_{10}\left(\frac{||\boldsymbol{E}_{\mathrm{ref}}| - |\boldsymbol{E}_{\mathrm{rec}}||}{\max(|\boldsymbol{E}_{\mathrm{ref}}|)}\right) \tag{41}$$

with respect to the fields $\boldsymbol{E}_{\mathrm{ref}}$ caused by the original dipole sources of the AUT that is provided. Probe correction with the true and the assumed probe behavior was performed, and a transformation without probe correction was done. The valid region of roughly $\varphi = \pm 80°$ is only achieved when employing the correct probe knowledge for correction. Despite the seemingly minor difference in the FF pattern of the true and the assumed probe, the transformed AUT radiation characteristic varies significantly between the two cases. In particular, the assumed probe and the Hertzian dipole, associated with no probe correction, do not contain the cross-polar component of the probe and considerable deviations with respect to the correct AUT pattern are visible in Fig. 5(b).

Figure 6 shows the performance of the nonconvex transformations with unknown probe coefficients. The optimization-based formulation and the alternating approach were allowed to run 15×10^3 and 5×10^3 iterations. As an initial guess, both solvers started from coefficients belonging to the assumed, nontilted probe. Since $m < n_{\mathrm{P}} n_{\mathrm{A}}$, the convex solver has not been employed. From the available number and type of measurements, both nonconvex techniques are not able to correctly

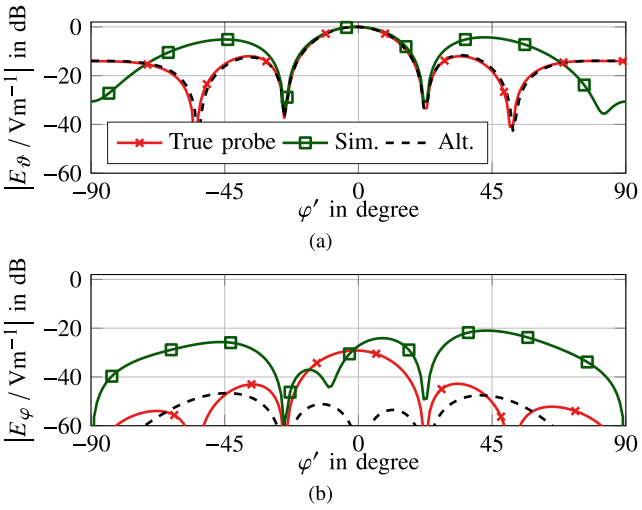

Fig. 7. Probe radiation patterns in the plane $\vartheta' = 90°$ retrieved as a by-product of the transformation results in Fig. 6 in comparison to the true probe characteristic. (a) Co-polar fields. (b) Cross-polar fields.

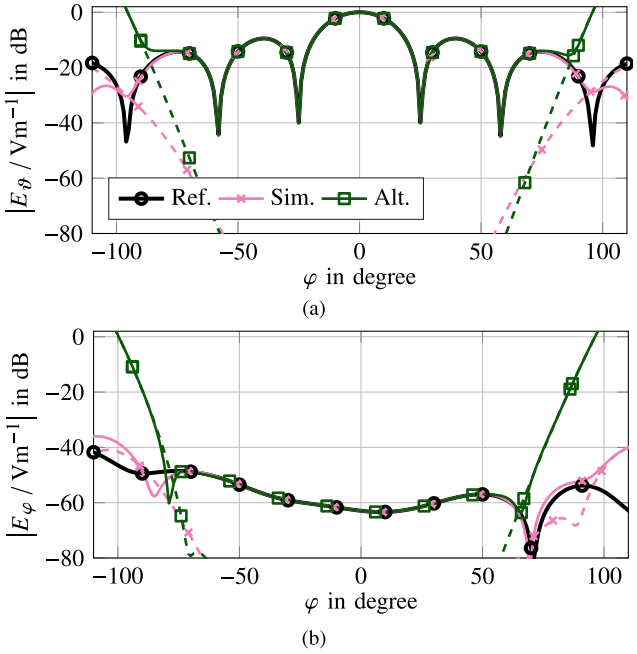

Fig. 8. AUT FF pattern for $\vartheta = 90°$ computed from planar NF measurements with four probe orientations ($\vartheta' = 90°, \varphi' = 0°, \mathcal{X}' \in \{0°, 90°\}$) and ($\vartheta' = 90°, \varphi' = 45°, \mathcal{X}' \in \{45°, 135°\}$). Transformation results for unknown probe coefficients, employing the nonconvex simultaneous optimization-based approach and the nonconvex alternating technique. (a) Co-polar fields. (b) Cross-polar fields. Dashed lines represent $\epsilon_{\mathrm{dB,FF}}$.

resolve the cross-polar field. However, the alternating method determines the co-polar component slightly more accurately as the transformation that falsely utilizes the nontilted probe pattern for the probe correction. The correspondingly reconstructed probe radiation characteristics are shown in Fig. 7. In accordance with the distortions in the cross-polarization of the AUT, the cross-polar behavior of the probe is not correctly obtained. However, the alternating approach does achieve a visually close match of the true probe in terms of the co-polar fields. In conclusion, classical planar NF measurements involving two probe polarizations (rotations) seem to be of moderate suitability for measurements and NFFFTs with unknown probe and AUT. Better results should be obtainable with more diverse measurements, e.g., involving more probe orientations.

b) Probe rotation around x' and z': At 289 measurement locations, the true probe antenna was placed with four different orientations defined via ($\vartheta' = 90°, \varphi' = 0°, \mathcal{X}' \in \{0°, 90°\}$) and ($\vartheta' = 90°, \varphi' = 45°, \mathcal{X}' \in \{45°, 135°\}$), resulting in $m = 1156$ available probe signals. This choice of probe orientations does involve four different polarization angles and two angles in the $x'y'$ plane—facing the AUT and looking past the AUT. The solver settings and the initial guesses were chosen identical to those in the previous scenario. For this more diverse probe arrangement, the results of the transformation when employing the falsely assumed probe pattern or no probe correction are almost identical to those presented in Fig. 5 and are, therefore, omitted. Figures 8 and 9 show the obtainable FF radiation characteristic of the AUT and the probe when employing the nonconvex methods. Again, no results for the convex approach based on bilinear forms are shown since $m < n_\mathrm{P} n_\mathrm{A}$. In fact, while the diversity in the measurement samples provided sufficient information for the two nonconvex approaches to return accurate results, the convex technique failed, even when employing a dense sampling grid with $m > n_\mathrm{P} n_\mathrm{A}$. This indicates that the rank($\boldsymbol{Q}^\mathrm{H}\boldsymbol{Q}$) has not yet

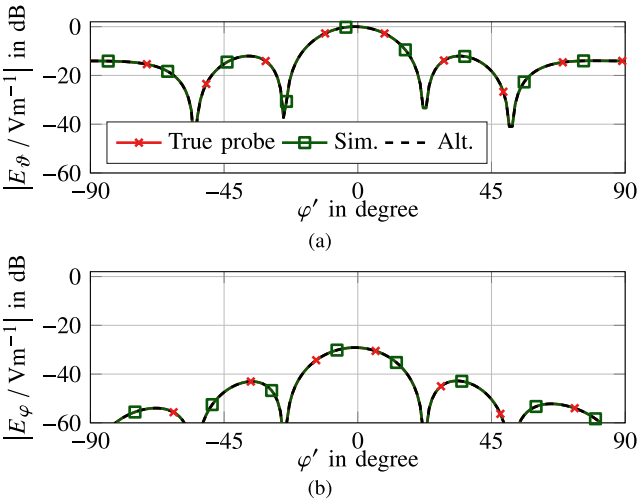

Fig. 9. Probe radiation patterns in the plane $\vartheta' = 90°$ retrieved as a by-product of the transformation results in Fig. 8 in comparison to the true probe characteristic. (a) Co-polar fields. (b) Cross-polar fields.

reached the necessary limit of $n_\mathrm{P} n_\mathrm{A}$ and that more information can still be obtained by more diverse measurements.

c) Randomly oriented probe: In order to further incorporate information about the probe into the measurement setup, random probe orientations in the range of $\vartheta' \in [0°, 180°]$, $\varphi' \in [0°, 360°]$, and $\mathcal{X}' \in [0°, 90°]$ were assumed. In total, $m = 9604$ probe signals were acquired such that the convex approach based on bilinear forms could be utilized. Results for the nonconvex optimization-based method and the convex technique are shown in Fig. 10, proving their potential for accurate transformations as soon as sufficiently diverse data

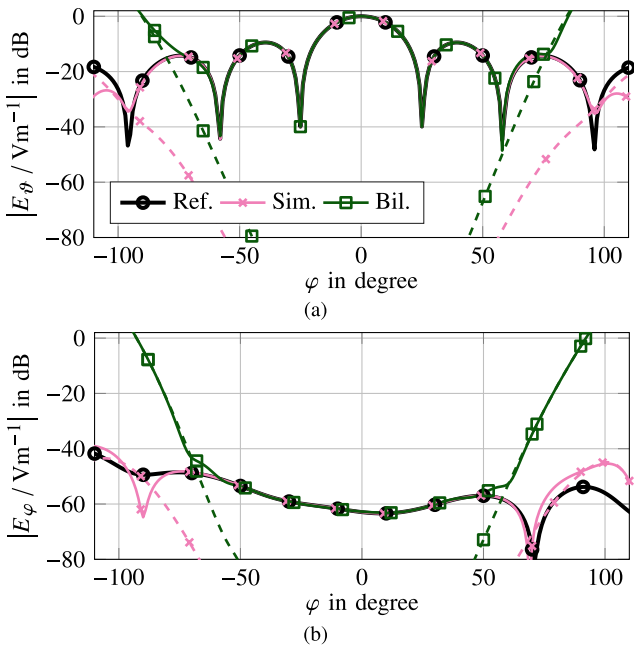

Fig. 10. AUT FF pattern for $\vartheta = 90°$ computed from planar NF measurements with randomized probe orientations. Transformation results for unknown probe coefficients, employing the nonconvex simultaneous optimization-based approach and the convex technique. (a) Co-polar fields. (b) Cross-polar fields. Dashed lines represent $\epsilon_{\mathrm{dB,FF}}$.

are available. Since the obtained FF patterns of the probe are visually identical to those of Fig. 9, they are not drawn. Also, the results obtained via the alternating method are similar to those of the simultaneous optimization and are not shown. Here, with more diversity in the probe arrangement, the convex solver seems to be able to accurately determine the AUT coefficients. However, note that the probe coefficients returned by Algorithm 1 were incorrect and that the rank condition was again not met. In fact, the rank (dependent on the truncation threshold) was in the range of 2000–3000 and, thus, would have been sufficient for an inverse-crime-based model with $n_\mathrm{A} = 200$ dipoles, however, not for the $n_\mathrm{A} = 336$ spherical vector wave functions. A rank in this transition region can potentially explain this partially accurate solution. Here and as a workaround, Algorithm 4 was applied in connection with (32) to retrieve the correct probe representation from the AUT coefficients returned from the convex solver. Still, for practical applications, the bilinear formulation seems to remain unfeasible.

3) Identical Probe and AUT: All four discussed methods can be applied to the particular case when AUT and probe are identical. This can be seen as a generalization of the two-antenna method [21] known from FF measurements, which has later, with restrictions, been generalized to NF measurements [23, pp. 93–98] [24], [25]. By enforcing the AUT and probe to be identical, one would hope for a less ill-posed inverse problem and mitigated requirements on the necessary measurement diversity. In order to have any chance of a successful transformation, $m \geq n_\mathrm{A}$ needs to be ensured at all times.

Algorithm 5 Alternating Probe and AUT Reconstruction when AUT and Probe are Identical (MATLAB Pseudocode)

Input: cell array `Ai` $= \boldsymbol{A}_i$, measurement vector `b` $= \boldsymbol{b}$, initial guess `z0` $= \boldsymbol{z}_{\mathrm{P0}} = \boldsymbol{z}_{\mathrm{A0}}$, iterations `k` $= k_\mathrm{it}$

Output: vector of coefficients `z` $= \boldsymbol{z}_\mathrm{A} = \boldsymbol{z}_\mathrm{P}$

```
z = z0;
for a = 1:k
    M ← Alg. 2 from z
    N ← Alg. 3 from z
    z = [M;N]\begin{align*}b(:);b(:)]
end
return z
```

An adaption of the nonconvex alternating approach is provided in Algorithm 5, for which the matrices $\boldsymbol{M}$ and $\boldsymbol{N}$ are constructed and employed in a linear system simultaneously. The number of measurements is doubled, while only one set of unknowns remains, effectively increasing the ratio of the number of measurements to unknowns. For the convex technique employing bilinear forms, fewer $\boldsymbol{P}_{ij}$ matrices can be utilized in the reconstruction process, and however, the size and effort involved in the matrix $\boldsymbol{Q}^\mathrm{H}\boldsymbol{Q}$ do not change. The computational effort is thus reduced, while a similar measurement diversity should be required. Finally, the nonconvex simultaneous implementation can directly force the probe to be identical with the AUT by removing the probe coefficients $\boldsymbol{z}_\mathrm{P}$ from the vector of unknowns $\boldsymbol{z}$ and having the matrix $\boldsymbol{O}_1$ duplicate the AUT unknowns $\boldsymbol{z}_\mathrm{A}$. With a reduced number of unknowns, the computational effort slightly reduces and fewer measurement samples are expected to be necessary for the algorithm to return accurate results.

a) Random data: Figure 11 shows the success rate of the three previously investigated algorithms and an implementation of the SDP formulation for the scenario of unknown and identical AUT and probe for randomly Gaussian distributed data. The modified versions of the convex technique and the nonconvex simultaneous method exploiting $\boldsymbol{z}_\mathrm{P} = \boldsymbol{z}_\mathrm{A}$ have been included. As expected, both convex algorithms featuring bilinear forms behave similarly, whereas the modified nonconvex simultaneous implementation requires fewer measurement samples due to halving of the number of unknowns. The convex approach based on SDP has here been implemented via the optimization framework described by (3) and (4). The solution is ensured to be positive definite by means of a Cholesky decomposition, similar to the implementation of a PhaseCut [99] variant in [100, Appendix A.7]. Its slightly lower success rate should be related to the approximations involved in the formulation, which are not necessary for the derivation of the nonconvex methods. In line with the discussion of Figs. 2 and 3, considerable nonzero success rates for $m < n_\mathrm{A}$, i.e., $m/n_\mathrm{A}^2 < 0.25$, are artificially caused by the small problem dimensions in connection with the inverse crime problem and the random starting points—however, the overall trend remains valid.

b) Measurement data at 40 GHz*:* Measurement data of a circular horn antenna at 40 GHz has been investigated. The planar measurement setup and a closer view on the horn

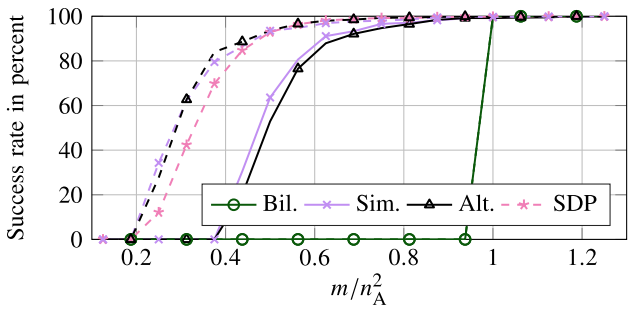

Fig. 11. Probe and AUT reconstruction for identical AUT and probe with $n_A = 4$ and randomly distributed data. For each sampling ratio, 10^3 simulations were run and success was declared once $\epsilon_{dB} \leq -60$ dB for the AUT coefficients was achieved. Dashed curves represent the results obtained by formulations explicitly exploiting $\boldsymbol{z}_P = \boldsymbol{z}_A$.

(a) (b)

Fig. 12. (a) Planar measurement setup of (b) circular horn AUT at 40 GHz. On the probe stage, an OEWG probe is mounted. Absorbers covering the mounting structure of the AUT have been removed for taking the picture.

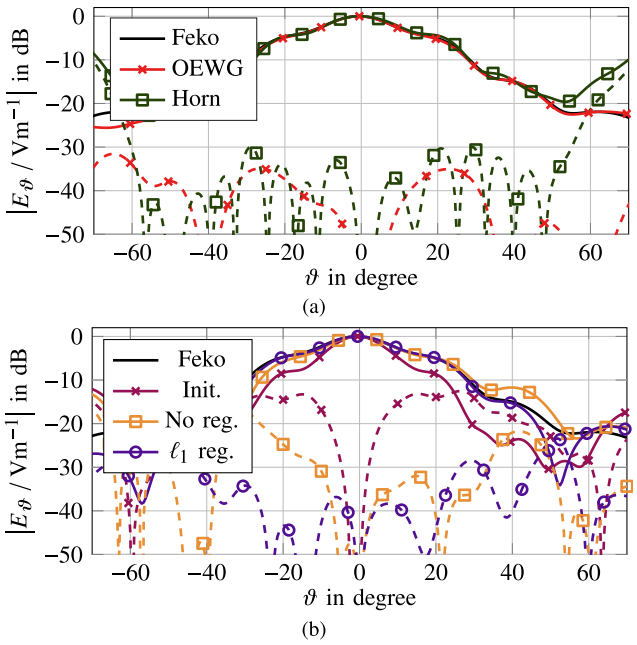

Fig. 13. Transformed FF of the horn antenna at 40 GHz. The co-polar field component in a vertical cut $\varphi = 90°$ through the main beam is shown. (a) Results with known probe corrections. (b) Initial guess for and results of the NFFFT with unknown probe coefficients. Dashed lines represent $\epsilon_{dB,FF}$.

antenna can be seen in Fig. 12. Two measurements with two different probe antennas have been performed, one utilizing an open-ended waveguide (OEWG) and a second employing an identical circular horn antenna as the probe. Two measurement planes of 47 cm × 28 cm were scanned at distances of 7.5 cm and 10 cm to the AUT. First, the measurement with the OEWG was processed where a probe correction based on a Feko [101] simulation of the OEWG was employed, and only measurements on the plane at $z = 10$ cm were exploited. Then, the determined source coefficients of the horn antenna were utilized for the probe correction of the second measurement. In addition, the simultaneous nonconvex NFFFT for unknown probes was applied to the dataset of the second measurement. As an equivalent model for the horn, $n = 394$ Hertzian dipoles placed tangentially on a circular disk covering the horn aperture were chosen. For the measurement data with the OEWG, a relative deviation, defined in (40), of around −39.0 dB between the measured and the reconstructed NF was obtained. When transforming data from both measurement surfaces, which has been acquired with the second horn, and employing a probe correction based on the sources found from the OEWG measurement, an NF deviation of −20.8 dB was observed. This decrease in accuracy is most likely to be attributed to the asymmetry of the measurement setup, which renders the radiation behavior of the horn antenna to be slightly different when being mounted on the probe stage instead of the AUT stage.

In Fig. 13(a), the transformation results of the first measurement with the OEWG probe with known probe correction via simulation data and the transformation of the second measurement, employing the measured horn behavior for probe correction, are shown. An estimated valid region of approximately ±50° is observable. For reference, the FF of a Feko simulation model of the horn antenna is drawn and the FF deviation of (41) between the measurements and the simulation model is evaluated. The co-polar field component in a vertical cut through the main beam is depicted ($\varphi = 90°$). Overall, the results for the OEWG probe and probe correction based on simulation data are observed to lead to a better agreement with the simulated horn behavior from Feko. The FF deviations in the co- and cross-polar fields are below −34 dB and −30 dB for the OEWG data and the horn data, respectively.

Figure 13(b) shows the FF reconstructed from the NF data acquired with the horn probe, where three transformations have been applied. First and as an initial guess for the simultaneous nonconvex transformation, results without any probe correction have been generated [labeled with “Init.” in Fig. 13(b)]. As expected, the radiation pattern is strongly distorted and exhibits a narrower main beam. Starting from these source coefficients, after 500 iterations the simultaneous nonconvex NFFFT, enforcing the AUT to be identical to the probe, returns the solution labeled as “No reg.”. In parts, this result seems to be more accurate, however, as not shown, it suffers from large deviations up to −4 dB in the cross-polar fields. A significantly improved accuracy is achieved by imposing an additional ℓ_1 regularization on the equivalent sources during the solution process, leading to convergence after 76 iterations with an NF deviation of −19.8 dB. As shown in Table I, this corresponds to a slightly larger NF deviation when compared to the results without regularization. However, regularization is crucial in order to suppress parasitic current contributions,

TABLE I
RELATIVE NF DEVIATIONS $\epsilon_{\mathrm{dB}}(\boldsymbol{Az}, \boldsymbol{A\hat{z}})$

OEWG	Horn	$\boldsymbol{z}_{\mathrm{A0}}$	No reg.	ℓ_1 reg.
−39.0 dB	−20.8 dB	−20.6 dB	−21.0 dB	−19.8 dB

specifically when working with noise-affected data and realistic AUT and probe models. Any superfluous degrees of freedom in the source representation of the probe may support parasitic AUT fields, which would not exist with an appropriate probe model. Mathematically speaking, the probe model can affect the null space of the associated probe-corrected forward operator. In this view, constraining the energy and number of contributing degrees of freedom of the probe limits the risk of reconstructing parasitic current distributions. For the considered example, the ℓ_1 regularization was seen to be better suited for this task than an ℓ_2 regularization and the result shown in Fig. 13(b) ("ℓ_1 reg.") exhibits an FF deviation of close to −30 dB in cross- and co-polar fields throughout most of the valid region.

Note that the obtained results were rather strongly dependent on the choice and weight of the regularization and that, up to now, no automatized and reliable procedure for defining the weight of the regularization has been identified. It is clear that an accurate solution can be found, but regularization is and will remain an extremely important key aspect of success.

IV. CONCLUSION

Common NFFFTs require the precise knowledge of the radiation behavior of the probe antenna, which is utilized for sampling the fields of the AUT. Missing or improper compensation of the influence of the probe—known as *probe correction*—deteriorates the quality of the determined AUT representation and, ultimately, the obtained FF pattern. Four NFFFT approaches were presented, which do not require knowledge of the electromagnetic properties of the probe antenna, but still consider its radiation characteristic and compensate its impact on the measurement. The different working principles of these algorithms were motivated by the close relationship of the problem with that of phaseless transformation algorithms. The discussed methods were observed to function well with randomly distributed data, which provides sufficient information about the probe and the AUT sources. Results obtained for simulation models of antenna NF measurements reveal issues for practical use cases, for example, when in common spherical measurement setups, the probe sources are always illuminated by the AUT from a single direction, making a unique determination of the probe coefficients difficult. Consistent with the experience with phaseless transformations, it was observed that the measurement setups for the simultaneous determination of AUT and probe need to be diversified to provide more information and constraints on the equivalent sources of AUT and probe. The problem is alleviated when utilizing two identical antennas as the AUT and the probe and, employing a suitable regularization, it was found to be solvable with decent accuracy for a typical planar measurement setup.

REFERENCES

[1] F. Jensen, "On the probe compensation for near-field measurements on a sphere," *AEÜ Int. J. Electron. Commun.*, vol. 29, pp. 305–308, 1975.

[2] D. Paris, W. Leach, and E. Joy, "Basic theory of probe-compensated near-field measurements," *IEEE Trans. Antennas Propag.*, vol. AP-26, no. 3, pp. 373–379, May 1978.

[3] E. Joy, W. Leach, and G. Rodrigue, "Applications of probe-compensated near-field measurements," *IEEE Trans. Antennas Propag.*, vol. AP-26, no. 3, pp. 379–389, May 1978.

[4] A. Yaghjian, "An overview of near-field antenna measurements," *IEEE Trans. Antennas Propag.*, vol. AP-34, no. 1, pp. 30–45, Jan. 1986.

[5] A. G. Repjar, A. C. Newell, and M. H. Francis, "Accurate determination of planar near-field correction parameters for linearly polarized probes," *IEEE Trans. Antennas Propag.*, vol. AP-36, no. 6, pp. 855–868, Jun. 1988.

[6] J. E. Hansen, *Spherical Near-Field Antenna Measurements*, vol. 26. Stevenage, U.K.: The Institute of Engineering and Technology, 2008.

[7] *1720-2012 - IEEE Recommended Practice for Near-Field Antenna Measurements*, Antennas and Propagation Society, Los Angeles, CA, USA, 2012.

[8] T. A. Laitinen, S. Pivnenko, and O. Breinbjerg, "Iterative probe correction technique for spherical near-field antenna measurements," *IEEE Antennas Wireless Propag. Lett.*, vol. 4, pp. 221–223, 2005.

[9] M. M. Leibfritz and P. M. Landstorfer, "Full probe-correction for near-field antenna measurements," in *Proc. 11th Symp. IEEE Antennas Propag. Soc. Int.*, Albuquerque, NM, USA, Jul. 2006, pp. 437–440.

[10] Y. Alvarez, F. Las-Heras, and M. R. Pino, "Probe distortion correction in near field–far field transformations based on equivalent sources characterization," in *Proc. 1st Eur. Conf. Antennas Propag.*, Nice, France, Nov. 2006, pp. 1–5.

[11] C. H. Schmidt, M. M. Leibfritz, and T. F. Eibert, "Fully probe-corrected near-field far-field transformation employing plane wave expansion and diagonal translation operators," *IEEE Trans. Antennas Propag.*, vol. 56, no. 3, pp. 737–746, Mar. 2008.

[12] R. Cornelius and D. Heberling, "Correction of non-ideal probe orientations for spherical near-field antenna measurements," in *Proc. 39th Symp. Antenna Meas. Techn. Assoc. Symp. (AMTA)*, Atlanta, GA, USA, Oct. 2017.

[13] A. C. Newell and S. F. Gregson, "Estimating the effect of higher order azimuthal modes in spherical near-field probe correction," in *Proc. 8th Eur. Conf. Antennas Propag. (EuCAP)*, Seattle, WA, USA, Apr. 2014, pp. 2486–2490.

[14] F. H. Larsen, "Probe correction of spherical near-field measurements," *Electron. Lett.*, vol. 13, no. 14, pp. 393–395, Jul. 1977.

[15] F. Saccardi, A. Giacomini, and L. J. Foged, "Comparative investigation of spherical NF measurements with full and first order probe correction using calibrated or simulated probe," in *Proc. 11th Eur. Conf. Antennas Propag. (EUCAP)*, Paris, France, Mar. 2017, pp. 3771–3775.

[16] M. A. Qureshi, C. H. Schmidt, and T. F. Eibert, "Probe pattern inaccuracy in fully probe corrected multilevel plane wave based near-field far-field transformed planar near-field measurements," in *Proc. 17th IEEE Int. Symp. Antennas Propag.*, Chicago, IL, USA, Jul. 2012, pp. 1–2.

[17] F. D'Agostino, F. Ferrara, C. Gennarelli, R. Guerriero, and M. Migliozzi, "Probe position errors corrected near-field-far-field transformation with spherical scanning," *Appl. Comput. Electromagn. Soc. J.*, vol. 31, no. 2, pp. 106–117, 2016.

[18] A. Newell, "Cross-polarization uncertainty in near-field probe correction [AMTA corner]," *IEEE Antennas Propag. Mag.*, vol. 51, no. 5, pp. 214–219, Oct. 2009.

[19] A. C. Newell, "Error analysis techniques for planar near-field measurements," *IEEE Trans. Antennas Propag.*, vol. AP-36, no. 6, pp. 754–768, Jun. 1988.

[20] P. Pelland, G. Hindman, and A. Newell, "Advances in automated error assessment of spherical near-field antenna measurements," in *Proc. 7th Eur. Conf. Antennas Propag.*, Gothenburg, Sweden, Nov. 2013, pp. 793–797.

[21] C. C. Cutler, A. P. King, and W. E. Kock, "Microwave antenna measurements," *Proc. IRE*, vol. 35, no. 12, pp. 1462–1471, Dec. 1947.

[22] *149–2021—IEEE Recommended Practice for Antenna Measurements*, Standards Antennas and Propagation Society, Logan, UT, USA, 2022.

[23] D. M. Kerns, *Plane-Wave Scattering-Matrix Theory of Antennas and Antenna-Antenna Interactions*. Gaithersburg, MD, USA: National Bureau of Standards, U.S. Department of Commerce, Jun. 1981.

[24] D. M. Kerns, "New method of gain measurement using two identical antennas," *Electron. Lett.*, vol. 6, no. 11, pp. 348–349, May 1970.

[25] G. K. Huddleston, E. B. Joy, G. P. Rodrigue, C. P. Burns, and W. J. Stoey, "A study of near-field data handling and probe design techniques," Georgia Inst. Technol., Atlanta, Georgia, Final Rep., Apr. 1976.

[26] R. C. Baird, A. C. Newell, P. F. Wacker, and D. M. Kerns, "Recent experimental results in near-field antenna measurements," *Electron. Lett.*, vol. 6, no. 11, pp. 349–351, May 1970.

[27] G. F. Masters, "Probe-correction coefficients derived from near-field measurements," in *Proc. 13th Antenna Meas. Techn. Assoc. Symp. (AMTA)*, Boulder, CO, USA, Oct. 1991, pp. 1–10.

[28] J. S. Hollis, T. Lyon, and L. Clayton, *Microwave Antenna Measurements*. Atlanta, GA, USA: Scientific-Atlanta, Jul. 1970.

[29] W. H. Kummer and E. S. Gillespie, "Antenna measurements—1978," *Proc. IEEE*, vol. 66, no. 4, pp. 483–507, Apr. 1978.

[30] C. A. Balanis, *Antenna Theory: Analysis and Design*, 3rd ed. Hoboken, NJ, USA: Wiley, 2005.

[31] A. C. Newell and D. M. Kerns, "Determination of both polarisation and power gain of antennas by a generalised 3-antenna measurement method," *Electron. Lett.*, vol. 7, no. 3, p. 68, 1971.

[32] A. Newell, R. Baird, and P. Wacker, "Accurate measurement of antenna gain and polarization at reduced distances by an extrapolation technique," *IEEE Trans. Antennas Propag.*, vol. AP-21, no. 4, pp. 418–431, Jul. 1973.

[33] P. F. Wacker, "Theory and numerical techniques for accurate extrapolation of near-zone antenna and scattering measurements," Nat. Bureau Standards, U.S. Dept. Commerce, Boulder, CO, USA, NBS Rep. 10 733, Apr. 1972.

[34] A. J. Yuffa, "On Wacker's essential equation in the extrapolation measurement technique," in *Proc. 41st Antenna Meas. Techn. Assoc. Symp. (AMTA)*, San Diego, CA, USA, Oct. 2019, pp. 1–5.

[35] S. Ishigami, H. Iida, and T. Iwasaki, "Measurements of complex antenna factor by the near-field 3-antenna method," *IEEE Trans. Electromagn. Compat.*, vol. 38, no. 3, pp. 424–432, Aug. 1996.

[36] H. Iida, S. Ishigami, I. Yokoshima, and T. Iwasaki, "Measurement of antenna factor of dipole antennas on a ground plane by 3-antenna method," *IEICE Trans. Commun.*, vol. 78, no. 2, pp. 260–267, Feb. 1995.

[37] *9.10.0.1602886 (r2021a)*, MATLAB, Natick, MA, USA, 2021.

[38] A. Paulus and T. F. Eibert, "Near-field far-field transformations with unknown probe antennas," in *Proc. 17th Eur. Conf. Antennas Propag.*, Florence, Italy, Mar. 2023l, pp. 1–11.

[39] J.-M. Jin, *Theory and Computation of Electromagnetic Fields*, 2nd ed. Piscataway, NJ and Hoboken, NJ, USA: IEEE Press, 2015.

[40] T. F. Eibert and C. H. Schmidt, "Multilevel fast multipole accelerated inverse equivalent current method employing Rao–Wilton–Glisson discretization of electric and magnetic surface currents," *IEEE Trans. Antennas Propag.*, vol. 57, no. 4, pp. 1178–1185, Apr. 2009.

[41] T. F. Eibert, E. Kilic, C. Lopez, R. A. Mauermayer, O. Neitz, and G. Schnattinger, "Electromagnetic field transformations for measurements and simulations," *Prog. Electromagn. Res.*, vol. 151, pp. 127–150, 2015.

[42] P. Petre and T. K. Sarkar, "Planar near-field to far-field transformation using an equivalent magnetic current approach," *IEEE Trans. Antennas Propag.*, vol. 40, no. 11, pp. 1348–1356, Nov. 1992.

[43] O. M. Bucci, C. Gennarelli, and C. Savarese, "Fast and accurate near-field-far-field transformation by sampling interpolation of plane-polar measurements," *IEEE Trans. Antennas Propag.*, vol. 39, no. 1, pp. 48–55, Jan. 1991.

[44] A. Bangun, C. Culotta-López, A. Behboodi, R. Mathar, and D. Heberling, "On phaseless spherical near-field antenna measurements," in *Proc. 13th Eur. Conf. Antennas Propag. (EuCAP)*, Mar. 2019, pp. 1–5.

[45] R. Pierri, G. D'Elia, and F. Soldovieri, "A two probes scanning phaseless near-field far-field transformation technique," *IEEE Trans. Antennas Propag.*, vol. 47, no. 5, pp. 792–802, May 1999.

[46] G. Schnattinger, C. Lopez, E. Kılıç, and T. F. Eibert, "Fast near-field far-field transformation for phaseless and irregular antenna measurement data," *Adv. Radio Sci.*, vol. 12, pp. 171–177, Nov. 2014.

[47] O. M. Bucci, G. D'Elia, and M. D. Migliore, "An effective near-field far-field transformation technique from truncated and inaccurate amplitude-only data," *IEEE Trans. Antennas Propag.*, vol. 47, no. 9, pp. 1377–1385, 1999.

[48] A. Bangun, A. Behboodi, and R. Mathar, "Signal recovery from phaseless measurements of spherical harmonics expansion," in *Proc. 27th Eur. Signal Process. Conf. (EUSIPCO)*, Sep. 2019, pp. 1–5.

[49] O. Breinbjerg and J. F. Álvarez, "Mathematical formulation of phase retrieval for phaseless spherical near-field antenna measurements with probe correction," in *Proc. URSI Int. Symp. Electromagn. Theory (EMTS)*, San Diego, CA, USA, May 2019, pp. 1–4.

[50] W. Wang, Y. Han, H. Gao, Y. Wu, Z. Lai, and Y. Liu, "An improved method of reducing SWE order for phaseless spherical near-field antenna measurement," *AEÜ Int. J. Electron. Commun.*, vol. 120, Jun. 2020, Art. no. 153199.

[51] A. Guth, C. Culotta-López, J. Maly, H. Rauhut, and D. Heberling, "Polyhedral sampling structures for phaseless spherical near-field antenna measurements," in *Proc. 42th Antenna Meas. Techn. Assoc. Symp. (AMTA)*, Newport, RI, USA, Nov. 2020.

[52] G. Alvarez-Narciandi et al., "Freehand system for antenna diagnosis based on amplitude-only data," *IEEE Trans. Antennas Propag.*, vol. 69, no. 8, pp. 4988–4998, Aug. 2021.

[53] T. Isernia, G. Leone, and R. Pierr, "Radiation pattern evaluation from near-field intensities on planes," *IEEE Trans. Antennas Propag.*, vol. 44, no. 5, pp. 701–710, May 1996.

[54] R. Pierri and R. Moretta, "On data increasing in phase retrieval via quadratic inversion: Flattening manifold and local minima," *IEEE Trans. Antennas Propag.*, vol. 68, no. 12, pp. 8104–8113, Dec. 2020.

[55] A. Paulus, J. Knapp, and T. F. Eibert, "Phaseless near-field far-field transformation utilizing combinations of probe signals," *IEEE Trans. Antennas Propag.*, vol. 65, no. 10, pp. 5492–5502, Oct. 2017.

[56] Y. Alvarez, F. Las-Heras, and M. R. Pino, "The sources reconstruction method for amplitude-only field measurements," *IEEE Trans. Antennas Propag.*, vol. 58, no. 8, pp. 2776–2781, Aug. 2010.

[57] F. Soldovieri, A. Liseno, G. D'Elia, and R. Pierri, "Global convergence of phase retrieval by quadratic approach," *IEEE Trans. Antennas Propag.*, vol. 53, no. 10, pp. 3135–3141, Oct. 2005.

[58] N. Mezieres, L. Le Coq, and B. Fuchs, "Spherical phaseless antenna measurements experimental validation of a two antenna positions procedure," *IEEE Antennas Wireless Propag. Lett.*, p. 1, 2022.

[59] Y. Saad and M. H. Schultz, "GMRES: A generalized minimal residual algorithm for solving nonsymmetric linear systems," *SIAM J. Sci. Stat. Comput.*, vol. 7, no. 3, pp. 856–869, Jul. 1986.

[60] C. C. Paige and M. A. Saunders, "LSQR: An algorithm for sparse linear equations and sparse least squares," *ACM Trans. Math. Softw.*, vol. 8, no. 1, pp. 43–71, Mar. 1982.

[61] R. W. Freund and N. M. Nachtigal, "QMR: A quasi-minimal residual method for non-Hermitian linear systems," *Numerische Math.*, vol. 60, no. 1, pp. 315–339, Dec. 1991.

[62] W. C. Chew, E. Michielssen, J. M. Song, and J.-M. Jin, *Fast and Efficient Algorithms in Computational Electromagnetics*. London, U.K.: Artech House, 2001.

[63] B. Carpentieri, I. S. Duff, L. Giraud, and G. Sylvand, "Combining fast multipole techniques and an approximate inverse preconditioner for large electromagnetism calculations," *SIAM J. Scientific Comput.*, vol. 27, no. 3, pp. 774–792, Jan. 2005.

[64] K. Zhao, M. N. Vouvakis, and J.-F. Lee, "The adaptive cross approximation algorithm for accelerated method of moments computations of EMC problems," *IEEE Trans. Electromagn. Compat.*, vol. 47, no. 4, pp. 763–773, Nov. 2005.

[65] J. Kornprobst, J. Knapp, R. A. M. Mauermayer, O. Neitz, A. Paulus, and T. F. Eibert, "Accuracy and conditioning of surface-source based near-field to far-field transformations," *IEEE Trans. Antennas Propag.*, vol. 69, no. 8, pp. 4894–4908, Aug. 2021.

[66] S. B. Adrian, A. Dély, D. Consoli, A. Merlini, and F. P. Andriulli, "Electromagnetic integral equations: Insights in conditioning and preconditioning," *IEEE Open J. Antennas Propag.*, vol. 2, pp. 1143–1174, 2021.

[67] T. F. Eibert, "Preconditioned inverse source solutions," in *Proc. 16th Eur. Conf. Antennas Propag. (EuCAP)*, Madrid, Spain, Mar. 2022, pp. 1–5.

[68] R. Moretta and R. Pierri, "Performance of phase retrieval via phaselift and quadratic inversion in circular scanning case," *IEEE Trans. Antennas Propag.*, vol. 67, no. 12, pp. 7528–7537, Dec. 2019.

[69] B. Fuchs, M. Mattes, S. Rondineau, and L. Le Coq, "Phaseless near-field antenna measurements from two surface scans—Numerical and experimental investigations," *IEEE Trans. Antennas Propag.*, vol. 68, no. 3, pp. 2315–2322, Mar. 2020.

[70] J. R. Fienup, "Phase retrieval algorithms: A comparison," *Appl. Opt.*, vol. 21, no. 15, pp. 2758–2769, Aug. 1982.
[71] R. W. Gerchberg, "A practical algorithm for the determination of phase from image and diffraction plane pictures," *Optik*, vol. 35, pp. 237–246, Sep. 1972.
[72] H. H. Bauschke, P. L. Combettes, and D. R. Luke, "Phase retrieval, error reduction algorithm, and Fienup variants: A view from convex optimization," *J. Opt. Soc. Amer. A, Opt. Image Sci.*, vol. 19, no. 7, pp. 1334–1345, Jul. 2002.
[73] V. Elser, "Phase retrieval by iterated projections," *J. Opt. Soc. Amer. A, Opt. Image Sci. Vis.*, vol. 20, no. 1, pp. 40–55, Jan. 2003.
[74] J. Sun, Q. Qu, and J. Wright, "A geometric analysis of phase retrieval," *Found. Comput. Math.*, vol. 18, no. 5, pp. 1131–1198, Oct. 2018.
[75] D. C. Liu and J. Nocedal, "On the limited memory BFGS method for large scale optimization," *Math. Program.*, vol. 45, nos. 1–3, pp. 503–528, Aug. 1989.
[76] N. Andrei, "Accelerated scaled memoryless BFGS preconditioned conjugate gradient algorithm for unconstrained optimization," *Eur. J. Oper. Res.*, vol. 204, no. 3, pp. 410–420, Aug. 2010.
[77] J. Nocedal and S. J. Wright, *Numerical Optimization*, 2nd ed. New York, NY, USA: Springer, 2006.
[78] W. Wirtinger, "Zur formalen theorie der funktionen von mehr komplexen Veränderlichen," *Mathematische Annalen*, vol. 97, no. 1, pp. 357–375, Dec. 1927.
[79] D. H. Brandwood, "A complex gradient operator and its application in adaptive array theory," *IEE Proc. H-Microw. Opt. Antennas*, vol. 130, no. 1, pp. 11–16, 1983.
[80] A. Van Den Bos, "Estimation of complex parameters," *IFAC Proc. Volumes*, vol. 27, no. 8, pp. 1429–1433, Jul. 1994.
[81] H. Li and T. Adalı, "Complex-valued adaptive signal processing using nonlinear functions," *EURASIP J. Adv. Signal Process.*, vol. 2008, no. 1, Dec. 2008, Art. no. 765615.
[82] W. H. Press, *Numerical Recipes in Fortran 77: The Art of Scientific Computing*, 2nd ed. Cambridge, U.K.: Cambridge Univ. Press, 2003.
[83] T. Isernia, G. Leone, and R. Pierri, "Phase retrieval of radiated fields," *Inverse Problems*, vol. 11, no. 1, pp. 183–203, Feb. 1995.
[84] A. J. Devaney and R. Chidlaw, "On the uniqueness question in the problem of phase retrieval from intensity measurements," *J. Optical Soc. Amer.*, vol. 68, no. 10, pp. 1352–1354, 1978.
[85] X. Ji, X. Liu, and B. Zhang, "Phaseless inverse source scattering problem: Phase retrieval, uniqueness and direct sampling methods," *J. Comput. Phys., X*, vol. 1, Jan. 2019, Art. no. 100003.
[86] T. Bendory, R. Beinert, and Y. C. Eldar, "Fourier phase retrieval: Uniqueness and algorithms," in *Compressed Sensing and Its Applications* (Applied and Numerical Harmonic Analysis), H. Boche, G. Caire, R. Calderbank, M. März, G. Kutyniok, and R. Mathar, Eds. Cham, Switzerland: Springer, 2017, pp. 55–91.
[87] J. H. Seldin and J. R. Fienup, "Numerical investigation of the uniqueness of phase retrieval," *J. Opt. Soc. Am. A*, vol. 7, no. 3, pp. 412–427, 1990.
[88] T. Isernia, F. Soldovieri, G. Leone, and R. Pierri, "On the local minima in phase reconstruction algorithms," *Radio Sci.*, vol. 31, no. 6, pp. 1887–1899, Nov. 1996.
[89] A. Conca, D. Edidin, M. Hering, and C. Vinzant, "An algebraic characterization of injectivity in phase retrieval," *Appl. Comput. Harmon. Anal.*, vol. 38, no. 2, pp. 346–356, Mar. 2015.
[90] B. G. Bodmann and N. Hammen, "Stable phase retrieval with low-redundancy frames," *Adv. Comput. Math.*, vol. 41, no. 2, pp. 317–331, Apr. 2015.
[91] R. Balan, P. Casazza, and D. Edidin, "On signal reconstruction without phase," *Appl. Comput. Harmon. Anal.*, vol. 20, no. 3, pp. 345–356, May 2006.
[92] A. Bandeira, J. Cahill, D. G. Mixon, and A. Nelson, "Fundamental limits of phase retrieval," in *Proc. 10th Int. Conf. Sampl. Theory Appl.*, Bremen, Germany, Jul. 2013, pp. 77–80.
[93] J. Milnor and D. Husemoller, *Symmetric Bilinear Forms*. Berlin, Germany: Springer, 1973.
[94] I. R. Shafarevich and A. O. Remizov, *Linear Algebra and Geometry*. Berlin, Germany: Springer, 2013.
[95] B. Cooperstein, *Advanced Linear Algebra*. Boca Raton, FL, USA: CRC Press, 2016.
[96] J. Knapp, A. Paulus, and T. F. Eibert, "Reconstruction of squared field magnitudes and relative phases from magnitude-only near-field measurements," *IEEE Trans. Antennas Propag.*, vol. 67, no. 5, pp. 3397–3409, May 2019.
[97] L. Vandenberghe and S. Boyd, "Semidefinite programming," *SIAM Rev.*, vol. 38, pp. 49–95, Apr. 1996.
[98] S. P. Boyd and L. Vandenberghe, *Convex Optimization*, 22nd ed. Cambridge, U.K.: Cambridge Univ. Press, 2018.
[99] I. Waldspurger, A. D'Aspremont, and S. Mallat, "Phase recovery, MaxCut and complex semidefinite programming," *Math. Program.*, vol. 149, nos. 1–2, pp. 47–81, Feb. 2015.
[100] A. H. Paulus, "Phaseless electromagnetic field transformations for magnitude-only and partially coherent field data," dissertation, Dept. Elect. Comput. Eng., Tech. Univ. Munich, Munich, Germany, 2022. [Online]. Available: http://nbn-resolving.de/urn/resolver.pl?urn:nbn:de:bvb:91-diss-20220531-1625304-1-3
[101] Altair Engineering Inc. (2018). *Altair Feko*. [Online]. Available: https://www.altair.com/feko/

Alexander Paulus (Member, IEEE) received the M.Sc. and Dr.-Ing. degrees in electrical engineering and information technology from the Technical University of Munich, Munich, Germany, in 2015 and 2022, respectively.

Since 2022, he has been working as a Senior Researcher at the Chair of High-Frequency Engineering, Department of Electrical and Computer Engineering, Technical University of Munich. His research interests include inverse electromagnetic problems, computational electromagnetics, and antenna measurement techniques.

Thomas F. Eibert (Senior Member, IEEE) received the Dipl.-Ing. (FH) degree from Fachhochschule Nürnberg, Nuremberg, Germany, in 1989, the Dipl.-Ing. degree from Ruhr-Universität Bochum, Bochum, Germany, in 1992, and the Dr.-Ing. degree from Bergische Universität Wuppertal, Wuppertal, Germany, in 1997, all in electrical engineering.

He is a Full Professor of high-frequency engineering with the Technical University of Munich, Munich, Germany, where he is currently the Academic Program Director responsible for the study courses in the Professional Profile Electrical and Computer Engineering.